

Differential senolytic inhibition of normal versus A β -associated cholinesterases: implications in aging and Alzheimer's disease

Sultan Darvesh^{1,2}, Meghan K. Cash¹, Katrina Forrestall¹, Hillary Maillet¹, Dane Sands¹

¹Department of Medical Neuroscience, Dalhousie University, Halifax, Nova Scotia B3H 4R2, Canada

²Department of Medicine (Geriatric Medicine and Neurology), Dalhousie University, Halifax, Nova Scotia B3H 2E1 Canada

Correspondence to: Sultan Darvesh; email: sultan.darvesh@dal.ca

Keywords: cellular senescence, β -amyloid, acetylcholinesterase, butyrylcholinesterase, cholinesterase inhibitors

Received: December 4, 2024

Accepted: March 13, 2025

Published: March 29, 2025

Copyright: © 2025 Darvesh et al. This is an open access article distributed under the terms of the [Creative Commons Attribution License](https://creativecommons.org/licenses/by/4.0/) (CC BY 4.0), which permits unrestricted use, distribution, and reproduction in any medium, provided the original author and source are credited.

ABSTRACT

Cellular senescence is a hallmark of aging and the age-related condition, Alzheimer's disease (AD). How senescence contributes to cholinergic and neuropathologic changes in AD remains uncertain. Furthermore, little is known about the relationship between senescence and cholinesterases (ChEs). Acetylcholinesterase (AChE) and butyrylcholinesterase (BChE) are important in neurotransmission, cell cycle regulation, and AD amyloid- β (A β) pathology. Senolytic agents have shown therapeutic promise in AD models. Therefore, we evaluated *in vitro* and *in silico* activity of senolytics, dasatinib (1), nintedanib (2), fisetin (3), quercetin (4), GW2580 (5), and nootropic, meclufenoxate hydrochloride (6), toward AChE and BChE. As ChEs associated with AD pathology have altered biochemical properties, we also evaluated agents 1-6 in AD brain tissues. Enzyme kinetics showed agents 1, 3, 4, and 6 inhibited both ChEs, while 2 and 5 inhibited only AChE. Histochemistry showed inhibition of A β plaque-associated ChEs (1 and 2: both ChEs; 5: BChE; 6: AChE), but not normal neural-associated ChEs. Modeling studies showed 1-6 interacted with the same five binding locations of both ChEs, some of which may be allosteric sites. These agents may exert their beneficial effects, in part, by inhibiting ChEs associated with AD pathology and provide new avenues for development of next-generation inhibitors targeting pathology-associated ChEs.

INTRODUCTION

The concept of cellular senescence was first used to describe diploid cells that ceased to proliferate [1]. Under normal conditions, cellular senescence has been suggested to be involved in maintaining tissue homeostasis during embryonic development, wound healing and repair, and suppression of tumor proliferation [2]. However, chronic accumulation of these cells can lead to deleterious effects. Cellular senescence is described as a hallmark of aging and age-related conditions such as Alzheimer's disease (AD) [2, 3].

Cellular senescence is identified by permanent cell cycle arrest and resistance to apoptosis in proliferative

cells such as astrocytes, microglia, oligodendrocytes, and endothelial cells [2]. It is independently regulated by the tumor suppressor p53/p21 and p16/pRB pathways [3] that result in preventing G₁ to S phase transition in the cell cycle [4, 5]. Cellular senescence is triggered by activation of harmful genes and sustained endogenous and exogenous stresses, including DNA and oxidative damage, telomere shortening, mitogenic and oncogenic signaling, mitochondrial dysfunction, and chromatin and lysosomal alterations [2].

Senescent cells are characterized by increased accumulation of the lysosomal enzyme senescence-associated- β -galactosidase [6] and lipofuscin [7], as well as the robust secretion of senescence-associated secretory phenotype (SASP) factors [8] including

activated inflammatory cytokines (e.g. interleukin 1 β (IL-1 β), interleukin 6 (IL-6), and tumor necrosis factor α (TNF α), chemokines, metalloproteinases, extracellular matrix components, and growth factors and regulators [2, 9]. Non-proliferative post-mitotic cells, like neurons, can also exhibit an increase in senescence-associated- β -galactosidase and lipofuscin. They also secrete SASP inflammatory factors [10], the hallmarks of senescence.

For more than 30 years, there has been an interest in the association between cognitive decline and cholinergic neurotransmission in aging, particularly in AD [11–13]. Regarding brain senescence, many facets of the cholinergic system, such as the neurotransmitter acetylcholine, synthesizing enzyme choline acetyltransferase (ChAT) and nicotinic and muscarinic acetylcholine receptors (nAChR and mAChR, respectively), have received great attention [14–18]. However, there have been few studies exploring the relationship between senescence and cholinesterases (ChEs) [18–23].

Acetylcholinesterase (AChE) and butyrylcholinesterase (BChE) are related serine hydrolases that co-regulate the cholinergic system through hydrolysis of acetylcholine [24, 25]. In the normal brain, BChE is primarily expressed in white matter, glia and distinct subcortical populations of neurons important for cognition and behavior while AChE is found in neurons and neuropil throughout the brain, with very little in white matter [24, 26, 27]. Although both ChEs share structural similarities [28] and functional homology [29], both AChE and BChE have distinct functions in health and disease beyond neurotransmission [25, 30].

In normal aging, there is a gradual decline in cholinergic function resulting in reduced levels of acetylcholine, ChAT, nAChRs, mAChRs, and AChE [31]. On the other hand, BChE activity has been shown to increase with age in the normal brain [32]. These changes have been correlated with age-related cognitive decline [11, 33]. In AD, pronounced cholinergic dysfunction is attributed to widespread loss of cholinergic neurons and significantly reduced acetylcholine levels that contribute to the salient cognitive and behavioural deficits characteristic of the disease [34, 35]. In turn, AChE levels are significantly reduced [36], while BChE levels remain the same [37] or increase [36, 38]. AChE and BChE are associated with the pathological hallmarks of AD, amyloid- β (A β) plaques and tau neurofibrillary tangles [39, 40], however, these enzymes are not associated with other dementia-related neuropathologies [41–43]. A role for BChE in the maturation of A β plaques, and consequently, AD progression [39] has been suggested due to its distinct association with the “malignant” fibrillar plaques of AD brains but not

the “benign” non-fibrillar plaques typically found in cognitively normal, aged brains [40, 41]. Plaque-bound ChEs appear to undergo a conformational change that alters their biochemical properties and differentiates these enzymes from those associated with normal neural elements [37, 44–46]. These biochemical changes lead to altered binding affinities [44, 47] and subsequent inhibitor sensitivities between ChEs associated with AD pathology and with normal neural elements [37, 44, 45]. Such alterations have significant implications in the design and development of potential next-generation therapeutic approaches targeting AChE and BChE for treatment of AD.

In addition to termination of cholinergic signaling, BChE is also involved in hydrolysis of the growth hormone secretagogue ghrelin, drug hydrolysis, lipid metabolism, detoxification of xenobiotics, and protein interaction and modification [25, 48, 49]. Moreover, both ChEs are also involved in cell proliferation and neural development [50, 51]. The non-cholinergic functions of AChE and BChE have been attributed to sharing similar sequence homologies of cell adhesion and ChE-like cell adhesion molecules [52, 53]. However, under pathological conditions, cell proliferation and apoptotic functions of ChEs appear altered. For instance, high levels of BChE activity and *BCHE* expression have been implicated in the rapid undifferentiated cellular proliferation of several brain tumor types [54, 55]. However, this rate of proliferation was reduced through the abolition of *BCHE* and BChE enzyme [55]. The *BCHE* gene has been shown to be upregulated in cell immortality in tumor development, whereby unchecked cell proliferation and evasion of cell death prevail, however, BChE suppression was shown to increase the rate of apoptotic processes [56].

Many approved and experimental cancer therapies are pro-apoptotic agents that exert their effects by targeting several intrinsic and extrinsic signaling pathways, including tumor suppressor pathways [57]. Furthermore, a number of these anti-cancer agents have been repurposed as senolytic agents as they also exhibit suppression of cellular senescence [58]. However, only a few senolytics have been identified as potential ChE inhibitors (ChEIs) [59, 60]. ChEIs that target AChE, BChE, or both [61], are a class of drugs that have been widely used for the treatment of several conditions, most notably the cognitive and behavioral symptoms associated with AD [62]. Several ChEIs, such as the AChE-selective donepezil and galantamine and the BChE-selective rivastigmine have shown to modulate apoptotic pathways and exert potent anti-inflammatory effects, in addition to their primary mode of action of increasing acetylcholine levels [63–65].

Cellular senescence is a significant contributor to low levels of chronic inflammation in normal aging, with notably increased levels of inflammatory cytokines in AD [2]. There is an established relationship between cholinergic function and immunomodulation [66–69]. Immune cells are equipped with the necessary cholinergic components, including ChAT, nAChRs and mAChRs, as well as AChE and BChE, required for modulation of cell activity through the cholinergic anti-inflammatory pathway (CAIP). ChEIs stimulate CAIP [70, 71], leading to decreases in macrophage and microglial secretion of pro-inflammatory cytokines such TNF α , IL-1 β , and IL-6 [66, 67, 72].

Senolytic agents such as dasatinib, nintedanib, fisetin, and quercetin and the nootropic, anti-aging agent meclofenoxate hydrochloride (also referred to as centrophenoxine) (Figure 1) have undergone or are currently undergoing human clinical trials in patients with age-related diseases [73–75]. They, along with the senolytic GW2580, have also had promising results in ameliorating inflammation, decreasing pathological load, and improving cognition in preclinical models of aging and AD [76–84]. However, the mechanism(s) by which senescent cells and their pro-inflammatory SASP factors contribute to aging and neurodegeneration, including neuropathology and dysfunction of the cholinergic system and CAIP is unknown. It has been suggested that increasing the bioavailability of acetylcholine for CAIP activation, via ChE inhibition, could be an attractive avenue for decreasing

neuroinflammation and modulating apoptotic activity in aging and AD [72, 85].

Because of the importance of ChEs in cell communication, the cell cycle, CAIP and AD neuropathology, we evaluated the enzyme kinetic properties of several senolytic and nootropic agents towards AChE and BChE to determine if they were inhibitors of these enzymes. In addition, since biochemical properties of ChEs associated with AD pathology are different from those associated with normal neural elements, using histochemical methods, we also evaluated whether these compounds inhibited ChEs that are associated with A β plaques in AD. We show that the selected senolytics and nootropic inhibit ChEs associated with plaques but not the enzymes associated with normal neural elements. Together, these findings suggest that these senolytic agents may exert their beneficial effects, in part, by inhibiting ChE-associated with A β pathology and providing new avenues for the development of the next generation of ChE inhibitors targeting AD pathology-associated ChEs.

RESULTS

Enzyme kinetic studies

To determine experimental inhibition constants (K_i values) and mode of inhibition for senolytic and nootropic compounds 1-6 with ChEs, Lineweaver-Burk

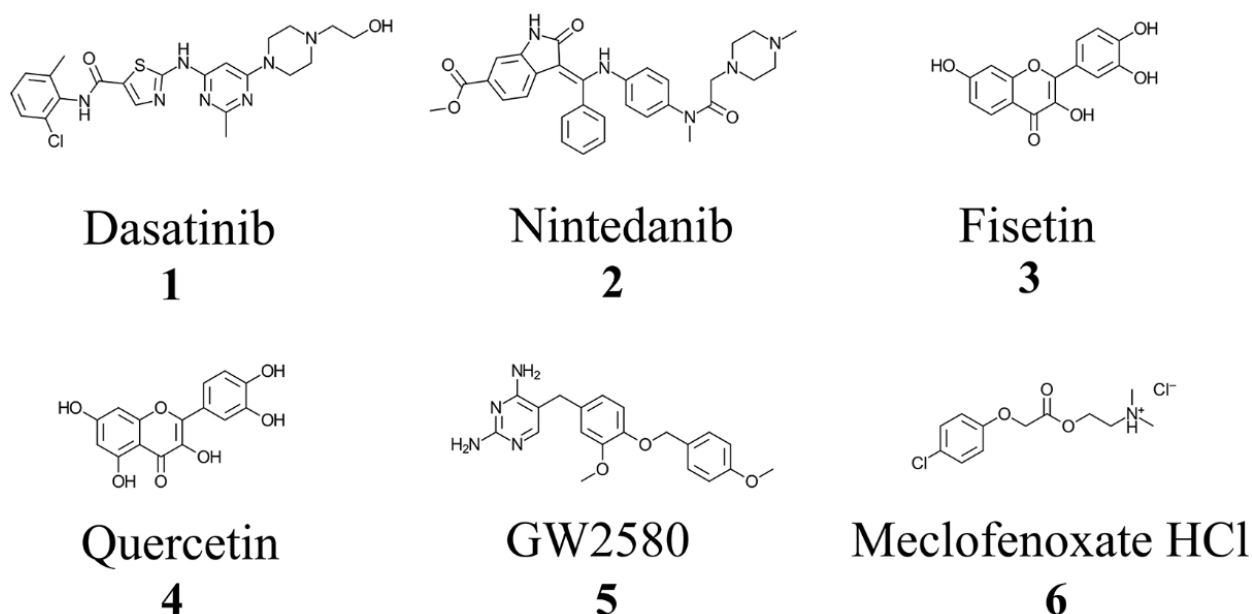


Figure 1. Chemical structures of approved and investigational senolytic (1-5) and nootropic (6) agents. Structures were drawn using ChemDoodle: 2D Chemical Drawing, Publishing and Informatics (Version 11.10, iChemLabs, LLC, Somerset, NJ, USA).

plots were generated (Figures 2, 3), as described previously [86]. Calculated experimental K_i values (μM) are shown in Table 1. Where ChE inhibition constants for compounds were identified previously in the literature [60, 87], K_i values observed herein were also similar (Table 1). All compounds showed some degree of ChE inhibition, except for 2 and 5 which did not inhibit BChE. Nintedanib (2) showed activity that was too low to conduct a full inhibition study.

Modes of inhibition were determined from Lineweaver-Burk plots, with most compounds showing mixed non-competitive inhibition, often indicative of allosteric binding – double reciprocal plot trendlines crossing

between x- and y-axes (Figures 2, 3). Fisetin (3) was the exception, showing robust competitive inhibition for AChE – trendlines crossing at the y-axis (Figure 2C), and clear uncompetitive inhibition with BChE – trendlines are parallel (Figure 3B). These results show that 3 outcompetes acetylthiocholine iodide (ATChI) for the active site of AChE; while 3 only targets the enzyme-butrylthiocholine iodide (BTChI) complex at which point it could bind to the active or allosteric sites to render inhibition of BChE. All other senolytic and nootropic agents are likely binding to only allosteric sites to produce the observed mixed non-competitive inhibitory responses.

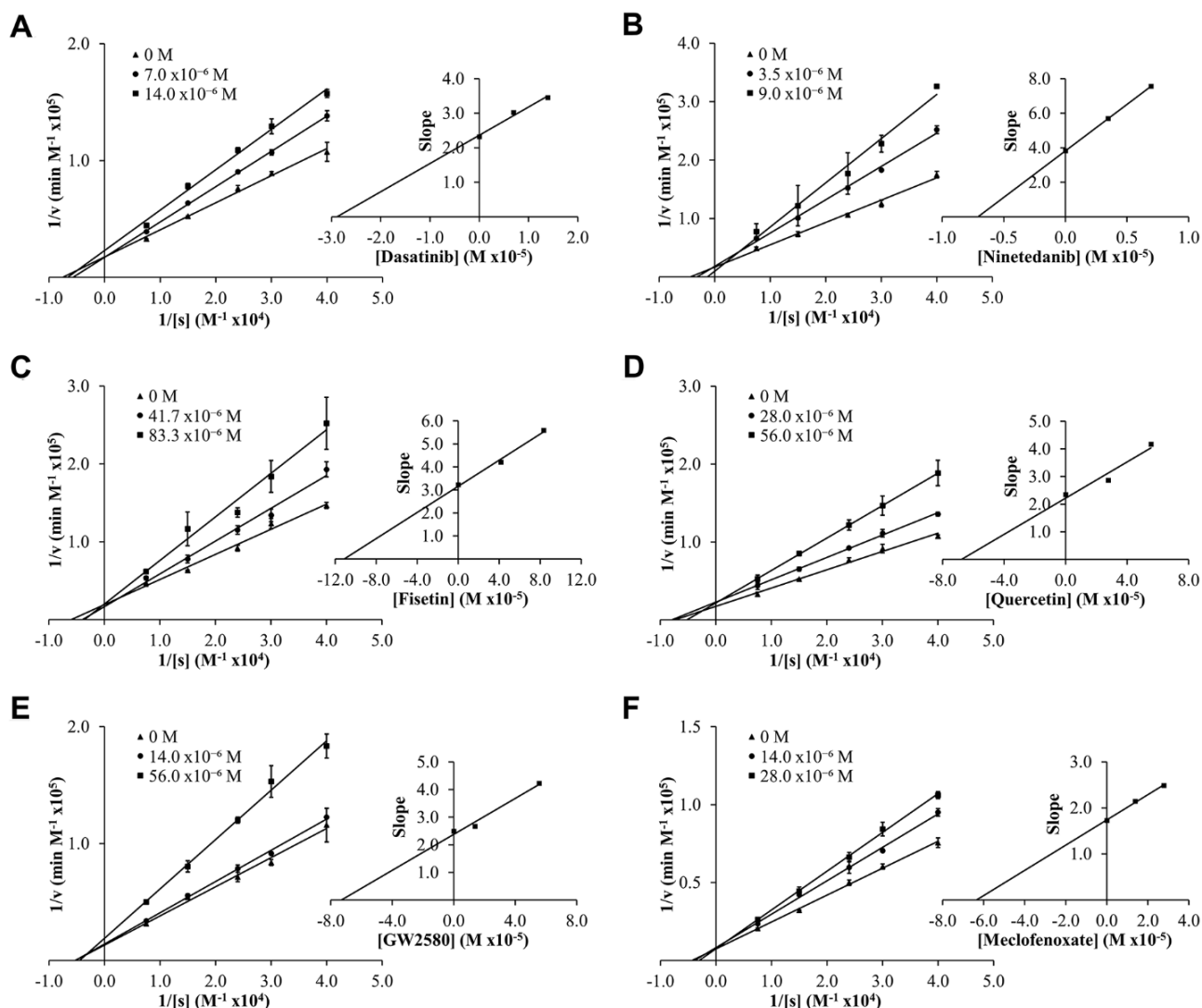


Figure 2. Lineweaver-Burk (LB) plots showing inhibition of acetylcholinesterase (AChE) upon treatment with varying concentrations of senolytic and nootropic agents 1-6 (A–F, respectively). Each compound was assessed at a range of concentrations (0–83 μM), with 0 M (▲), middle concentration (●), and highest concentration (■). Slopes from LB plot trendlines were plotted against compound concentrations to generate K_i values as the x-intercept (insert graphs). Enzyme kinetic experiments were performed in triplicate and kinetic parameter values were averaged.

Histochemical studies

Of the AD brains selected for this study (Table 2), three cases were previously described to have robust A β -, AChE-, and BChE-associated plaque loads in the cerebral cortex [42, 46, 88]. The fourth case, BB11-010, also showed severe AD and ChE-associated pathology, consistent with the other selected cases.

Histochemical staining was done at pH 6.8 to allow for the visualization of ChE activity associated with plaques, while pH 8.0 was used to visualize ChE activity associated with normal neural elements, as shown previously [37, 88]. The staining quality of ChEs in tissues selected for this study were examined using the standard Karnovsky-Roots (KR) substrate staining method and found to be appropriate prior to treatment with compounds 1-6.

The use of senolytic and nootropic compounds 1-6 in KR histochemical staining resulted in varying degrees of inhibition of AChE and BChE activity associated with normal neural elements (pH 8.0) and plaques (pH 6.8) in human AD brain tissues, ranging from no inhibition (-) to strong inhibition (xxx). Qualitative

analysis of each of the four AD cases selected is described as the average rankings for each compound in Table 3. Representative photomicrographs showing AChE and BChE histochemical staining of AD brain tissues with or without treatment with compounds 1-6 are shown in Figures 4–9.

In the presence of compound 1, AChE staining associated with plaques was reduced by varying degrees when compared with control staining at pH 6.8 (Table 3 and Figure 4A, 4B). While two of the AD cases showed complete inhibition of AChE-associated plaques, the remaining cases only showed moderate reduction in staining. Compound 1 showed complete inhibition of BChE activity associated with plaques in all cases, although white matter staining remained when compared to control staining at pH 6.8 (Table 3 and Figure 4E, 4F). There was no inhibition of AChE or BChE staining associated with normal neural elements (pH 8.0) in any cases, relative to controls, when treated with compound 1 (Figure 4C, 4D, 4G, 4H).

Similarly, complete inhibition of both AChE and BChE activity associated with plaques, compared to controls, was observed in the presence of compound 2

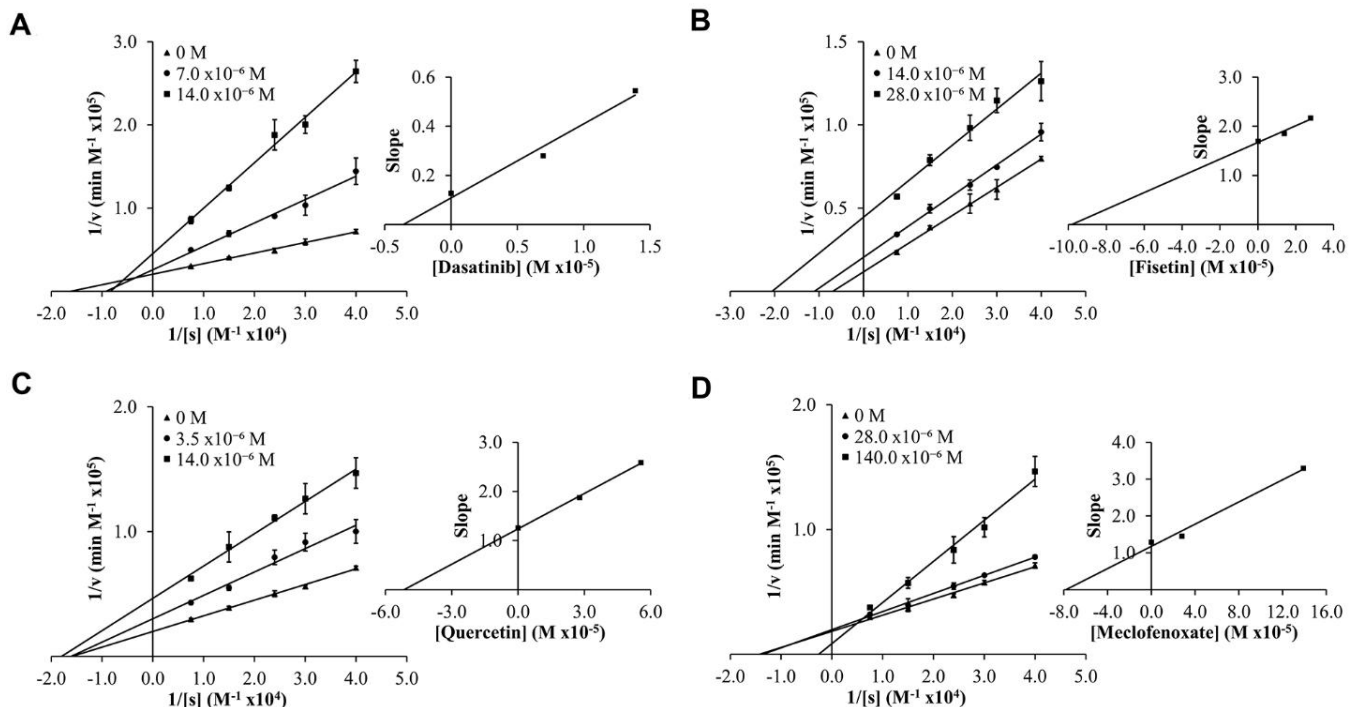


Figure 3. Lineweaver-Burk (LB) plots showing inhibition of butyrylcholinesterase (BChE) upon treatment with varying concentrations of senolytic and nootropic agents 1, 3, 4 and 6 (A–D, respectively). Compounds 2 and 5 showed too little inhibition to complete LB kinetics. Each compound was assessed at a range of concentrations (0–140 μ M), with 0 M (▲), middle concentration (●), and highest concentration (■). Slopes from LB plot trendlines were plotted against compound concentrations to generate K_i values as the x-intercept (insert graphs). Enzyme kinetic experiments were performed in triplicate and kinetic parameter values were averaged.

Table 1. Experimental inhibition constants (K_i values) and mode of inhibition for compounds 1-6 with acetylcholinesterase (AChE) and butyrylcholinesterase (BChE).

Compound	Experimental AChE K_i (μ M) (Mode of inhibition)	Experimental BChE K_i (μ M) (Mode of inhibition)
	Literature AChE K_i values	Literature BChE K_i values
Dasatinib (1)	28.22 (Mixed Non-competitive)	3.36 (Mixed Non-competitive)
Nintedanib (2)	7.10 (Mixed Non-competitive)	No Inhibition
Fisetin (3)	109.81 (Competitive)	94.35 (Uncompetitive)
Quercetin (4)	100.2 ^a	94.2 ^a
	62.19 (Mixed Non-competitive)	51.49 (Mixed Non-competitive)
GW2580 (5)	38.3 ^a , 76.2 ^b	68.0 ^a , 46.8 ^b
	70.97 (Mixed Non-competitive)	No Inhibition
Meclofenoxate Hydrochloride (6)	63.20 (Mixed Non-competitive)	76.30 (Mixed Non-competitive)

^a K_i values taken from Katalinić et al. [60].

^b K_i values taken from Orhan et al. [87].

Table 2. Demographic information for Alzheimer's disease (AD) brain tissues used.

Case #	Neuropathological diagnosis	Sex	Age (y)	Brain weight (g)	Braak stage	CERAD ^a plaque score
BB11-010	AD	M	93	1254	IV	Frequent
BB11-026	AD	M	98	1066	V	Frequent
BB11-039	AD	F	92	1009	IV	Frequent
BB12-035	AD	F	84	1120	VI	Frequent

^aCERAD, Consortium to Establish a Registry for Alzheimer's Disease.

(Figure 5A, 5B, 5E, 5F). There was no inhibition of ChE staining associated with normal neural elements (Table 3 and Figure 5C, 5D, 5G, 5H).

The two flavonoids, compounds 3 and 4, produced identical results under KR histochemical conditions (Table 3 and Figures 6, 7). When the aqueous stock solutions of 3 and 4 were added to their KR staining solutions, there were noticeable color and solubility changes from the original stocks. The stock solution of compound 3 was a cloudy, peach color, which turned umber and precipitated upon addition to the KR solution. The stock solution of compound 4 was a cloudy, neon yellow color, which turned brown and likewise precipitated when added to the KR solution. These observations indicated that the lack of ChE staining at pH 6.8 and 8.0 for tissues tested with

compounds 3 and 4 (Figures 6, 7) were likely due to both flavonoids forming complexes with metal ions of the KR solution, iron and/or copper [89, 90], necessary for the staining reaction to occur. Thus, producing the false impression of inhibitory activity.

Compound 5 did not inhibit staining of AChE associated with plaques; however, it did inhibit staining of BChE associated with plaques when compared to control staining (Table 3 and Figure 8A, 8B, 8E, 8F). Furthermore, compound 5 did not inhibit either ChE associated with normal neural elements compared to controls (Table 3 and Figure 8C, 8D, 8G, 8H).

Lastly, compound 6 showed moderate to strong inhibition of AChE-associated plaque staining and slight inhibition of BChE-associated plaque

Table 3. Qualitative analysis of senolytic and nootropic compound inhibition of Karnovsky-Roots staining for acetylcholinesterase (AChE) and butyrylcholinesterase (BChE) associated with β -amyloid plaques (pH 6.8) and normal neural elements (pH 8.0) in human orbitofrontal cortex and thalamus Alzheimer's disease brain tissues.

Senolytic compound	Staining results			
	AChE pH 6.8	BChE pH 6.8	AChE pH 8.0	BChE pH 8.0
Dasatinib (1)	xx/x ^a	xxx	-	-
Nintedanib (2)	xxx	xxx	-	-
Fisetin (3)	See below ^b	See below ^b	See below ^b	See below ^b
Quercetin (4)	See below ^b	See below ^b	See below ^b	See below ^b
GW2580 (5)	-	x/xx	-	-
Meclofenoxate Hydrochloride (6)	xx/x	x	-	-

^aThe inhibition in AChE or BChE staining resulting from senolytic and nootropic compound competition was categorized as: – (no inhibition), x (slight inhibition), xx (moderate inhibition), or xxx (strong inhibition).

^bThe presence of these compounds in the reaction mixture led to the chelation and precipitation of metal ions necessary for the Karnovsky-Roots method. Thus, histochemical staining could not be done.

staining when compared to control staining for AChE and BChE, respectively (Figure 9A, 9B, 9E, 9F). Although reduced, the appearance of AChE inhibition associated with plaques varied when comparing all AD cases. Cases with a relatively higher plaque burden appeared to have less reduction in ChE staining than cases with a relatively lower plaque burden. When comparing appropriate control sections to those stained in the presence of compound 6, the degree of inhibition remained the same in amongst all cases (not shown). Compound 6 did not inhibit AChE or BChE staining associated with normal neural elements (Table 3 and Figure 9C, 9D, 9G, 9H).

Molecular docking studies

Cholinesterase inhibitors are known to bind to varying sites on ChEs to yield effects on catalytic activity. *In silico* molecular docking studies provide a means of assessing potential enzyme binding sites and amino acid residue interactions that could contribute to the observed activity of compounds. As such, understanding the structural characteristics and features of AChE and BChE is essential to appropriately investigate the potential mechanisms of action for active compounds. Structural features of ChEs used to analyze molecular docking studies were based on the published x-ray crystal structures of these enzymes [91, 92].

AChE and BChE possess many of the same structural components and similar amino acid residues that are essential for catalytic activity. Though the volume of the active site gorge and the diameter of the gorge opening are larger in BChE than in AChE (~500 Å³ vs.

~300 Å³, ~16 Å vs. ~11 Å) [93], they both have a similar depth of ~20 Å and contain the same five main active site regions with key residues and structural features (acyl loop, Ω -loop, ϵ -helix) shown in Figure 10. These five regions include: 1) the catalytic active site (CAS) at the base of the gorge, comprised of the catalytic triad, serine (S203 for AChE, S198 for BChE), histidine (H447, H438), and glutamate (E334, E325); 2) the acyl binding pocket (ABP) at the mouth of the gorge; 3) the peripheral anionic site (PAS) at the mouth of the gorge; 4) the π -cationic site (PCS) midway down the gorge; and 5) the oxyanion hole (OAH) next to the catalytic serine at the bottom of the gorge (Supplementary Figure 1).

In addition to the main active site gorge, there are several proposed sites that are entry/exit routes for substrates and hydrolysis products that surround and share some residues of the active site gorge, the acyl and Ω -loops, and the ϵ -helix. These sites are denoted as the acyl, side, and back doors (Figure 10A) [94–97]. The discovery of the back door was originally hypothesized as an alternate exit route for choline from the active site of AChE following the hydrolysis of acetylcholine, and offered a possible explanation for its high turnover rate despite the restricted opening of the active site gorge [97]. The side and acyl doors were later proposed as additional entry/exit points to the gorge (Figure 10A) [94, 96, 98]. While these “doors” have not been described in detail in the literature for BChE, their key residues and structural components are likewise present in the BChE structure (Figure 10B), with many of the residues conserved between the two enzymes.

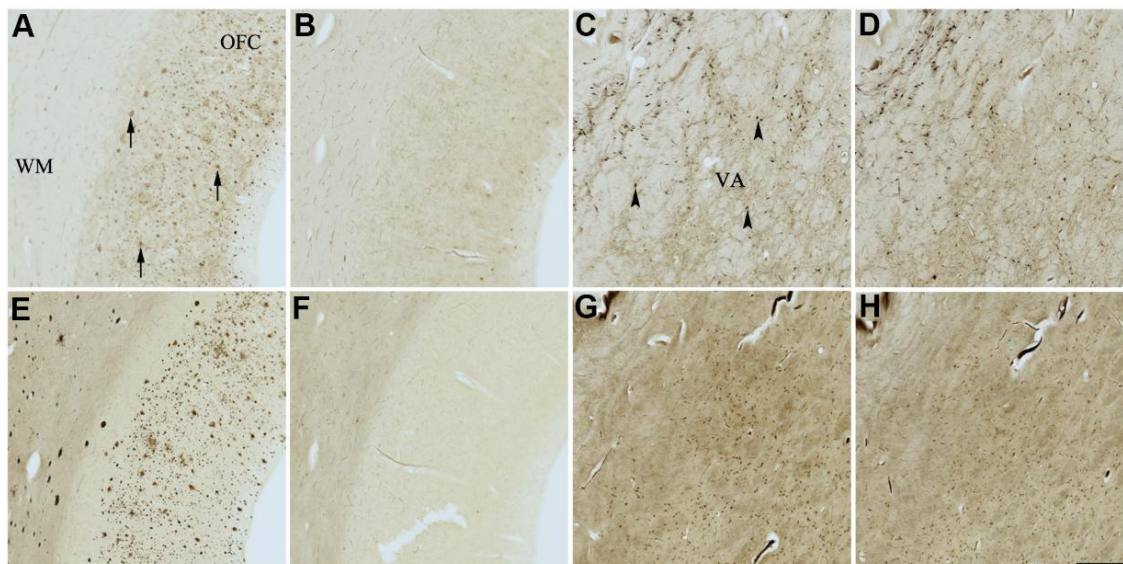


Figure 4. Effect of dasatinib (1) on histochemical staining of acetylcholinesterase (AChE) and butyrylcholinesterase (BChE). Representative photomicrographs of histochemical staining of AChE (A–D) and BChE (E–H). Staining at pH 6.8 demonstrates AChE- (A) and BChE (E)-associated plaques in the Alzheimer’s disease (AD) orbitofrontal cortex (arrows). Staining at pH 8.0 demonstrates AChE (C) and BChE (G) associated with normal neural structures in the AD thalamus (arrowheads showing neurons). Dasatinib (1) inhibits AChE (B) and BChE (F) associated with AD plaques but not AChE (D) and BChE (H) associated with normal neural elements. Note, for ease of reference, identical images of the positive control staining of AChE and BChE at pH 6.8 and 8.0 (A, C, E, G) were used herein and in Figures 5-9 (A, C, E, G) to help compare directly the effects of each senolytic or nootropic agent on the standard Karnovsky-Roots (KR) histochemical staining method. Abbreviations: OFC, orbitofrontal cortex; VA, ventroanterior thalamic nucleus; WM, white matter. Scale bar = 500 μ m.

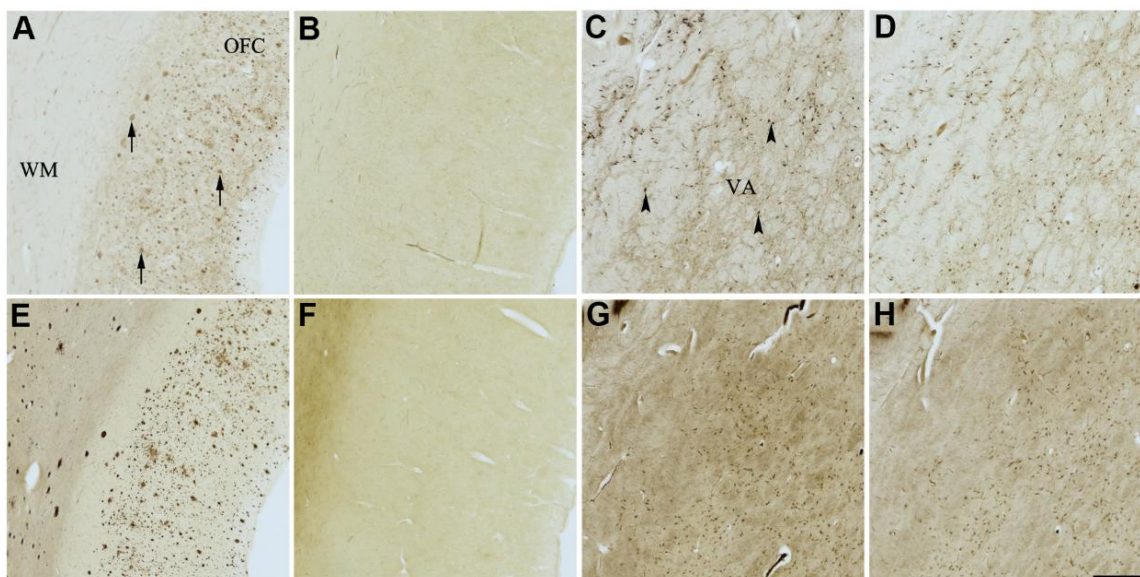


Figure 5. Effect of nintedanib (2) on histochemical staining of acetylcholinesterase (AChE) and butyrylcholinesterase (BChE). Representative photomicrographs of histochemical staining of AChE (A–D) and BChE (E–H). Staining at pH 6.8 demonstrates AChE- (A) and BChE (E)-associated plaques in the Alzheimer’s disease (AD) orbitofrontal cortex (arrows). Staining at pH 8.0 demonstrates AChE (C) and BChE (G) associated with normal neural structures in the AD thalamus (arrowheads showing neurons). Nintedanib (2) inhibits AChE (B) and BChE (F) associated with AD plaques but not AChE (D) and BChE (H) associated with normal neural elements. Note, for ease of reference, identical images of the positive control staining of AChE and BChE at pH 6.8 and 8.0 (A, C, E, G) were used herein and in Figures 4, 6–9 (A, C, E, G) to help compare directly the effects of each senolytic or nootropic agent on the standard Karnovsky-Roots (KR) histochemical staining method. Abbreviations: OFC, orbitofrontal cortex; VA, ventroanterior thalamic nucleus; WM, white matter. Scale bar = 500 μ m.

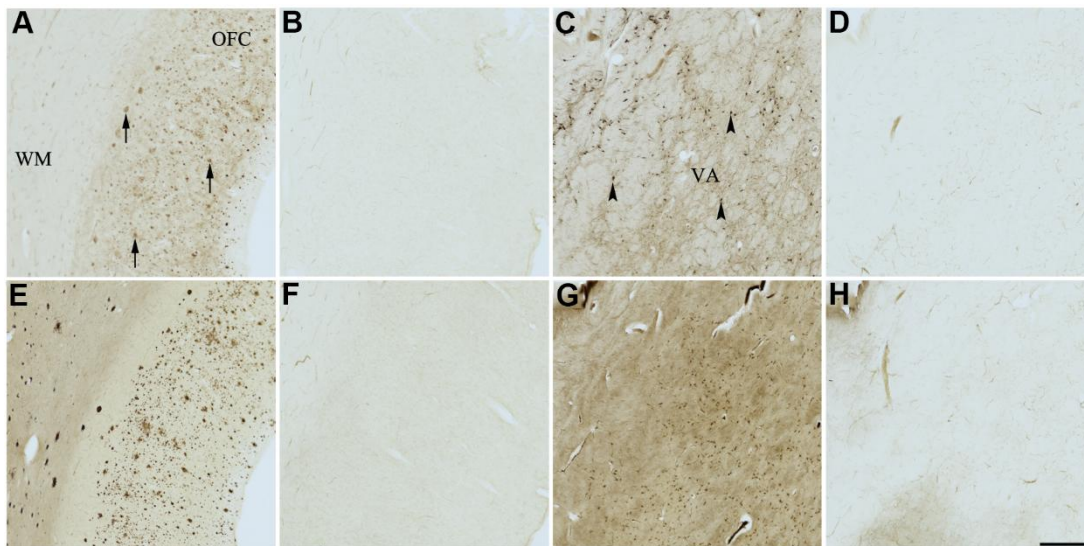


Figure 6. Effect of fisetin (3) on histochemical staining of acetylcholinesterase (AChE) and butyrylcholinesterase (BChE). Representative photomicrographs of histochemical staining of AChE (A–D) and BChE (E–H). Staining at pH 6.8 demonstrates AChE- (A) and BChE (E)-associated plaques in the Alzheimer’s disease (AD) orbitofrontal cortex (arrows). Staining at pH 8.0 demonstrates AChE (C) and BChE (G) associated with normal neural structures in the AD thalamus (arrowheads showing neurons). Staining reactions for AChE and BChE at pH 6.8 (B and F) or pH 8.0 (D and H) in the presence of fisetin (3) could not be done due to compound 3 precipitating out of solution, most likely due to chelating with metal ions required for the Karnovsky-Roots (KR) staining method. Note, for ease of reference, identical images of the positive control staining of AChE and BChE at pH 6.8 and 8.0 (A, C, E, G) were used herein and in Figures 4, 5, 7–9 (A, C, E, G) to help compare directly the effects of each senolytic or nootropic agent on the standard KR histochemical staining method. Abbreviations: OFC, orbitofrontal cortex; VA, ventroanterior thalamic nucleus; WM, white matter. Scale bar = 500 μ m.

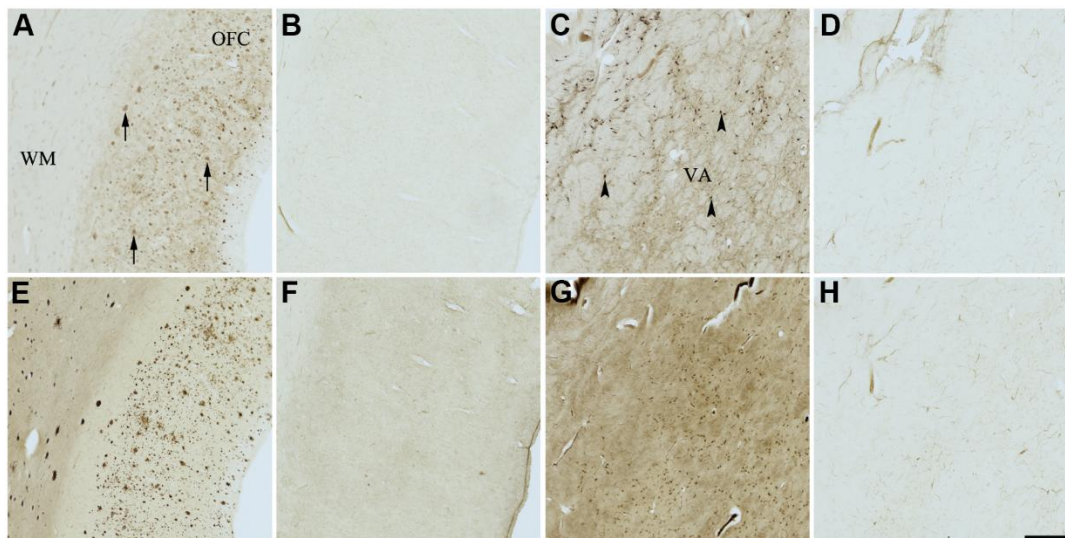


Figure 7. Effect of quercetin (4) on histochemical staining of acetylcholinesterase (AChE) and butyrylcholinesterase (BChE). Representative photomicrographs of histochemical staining of AChE (A–D) and BChE (E–H). Staining at pH 6.8 demonstrates AChE- (A) and BChE (E)-associated plaques in the Alzheimer’s disease (AD) orbitofrontal cortex (arrows). Staining at pH 8.0 demonstrates AChE (C) and BChE (G) associated with normal neural structures in the AD thalamus (arrowheads showing neurons). Staining reactions for AChE and BChE at pH 6.8 (B and F) or pH 8.0 (D and H) in the presence of quercetin (4) could not be done due to compound 4 precipitating out of solution, most likely due to chelating with metal ions required for the Karnovsky-Roots (KR) staining method. Note, for ease of reference, identical images of the positive control staining of AChE and BChE at pH 6.8 and 8.0 (A, C, E, G) were used herein and in Figures 4–6, 8, 9 (A, C, E, G) to help compare directly the effects of each senolytic or nootropic agent on the standard BChE KR histochemical staining method. Abbreviations: OFC, orbitofrontal cortex; VA, ventroanterior thalamic nucleus; WM, white matter. Scale bar = 500 μ m.

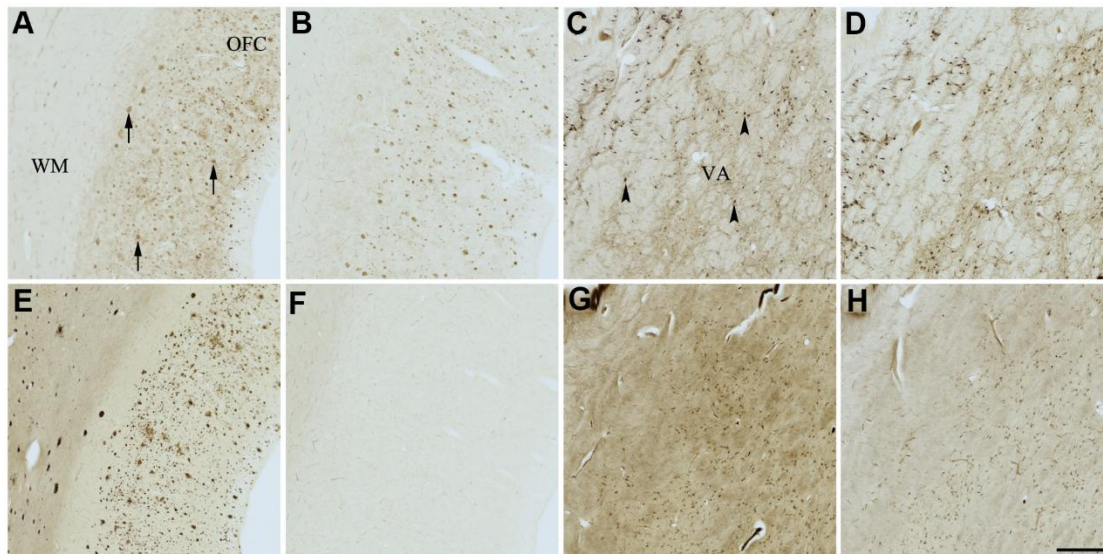


Figure 8. Effect of GW2580 (5) on histochemical staining of acetylcholinesterase (AChE) and butyrylcholinesterase (BChE). Representative photomicrographs of histochemical staining of AChE (A–D) and BChE (E–H). Staining at pH 6.8 demonstrates AChE- (A) and BChE (E)-associated plaques in the Alzheimer’s disease (AD) orbitofrontal cortex (arrows). Staining at pH 8.0 demonstrates AChE (C) and BChE (G) associated with normal neural structures in the AD thalamus (arrowheads showing neurons). GW2580 (5) inhibits BChE (F) but not AChE (B) associated with AD plaques but not AChE (D) and BChE (H) associated with normal neural elements. Note, for ease of reference, identical images of the positive control staining of AChE and BChE at pH 6.8 and 8.0 (A, C, E, G) were used herein and in Figures 4–7, 9 (A, C, E, G) to help compare directly the effects of each senolytic or nootropic agent on the standard Karnovsky-Roots (KR) histochemical staining method. Abbreviations: OFC, orbitofrontal cortex; VA, ventroanterior thalamic nucleus; WM, white matter. Scale bar = 500 μ m.

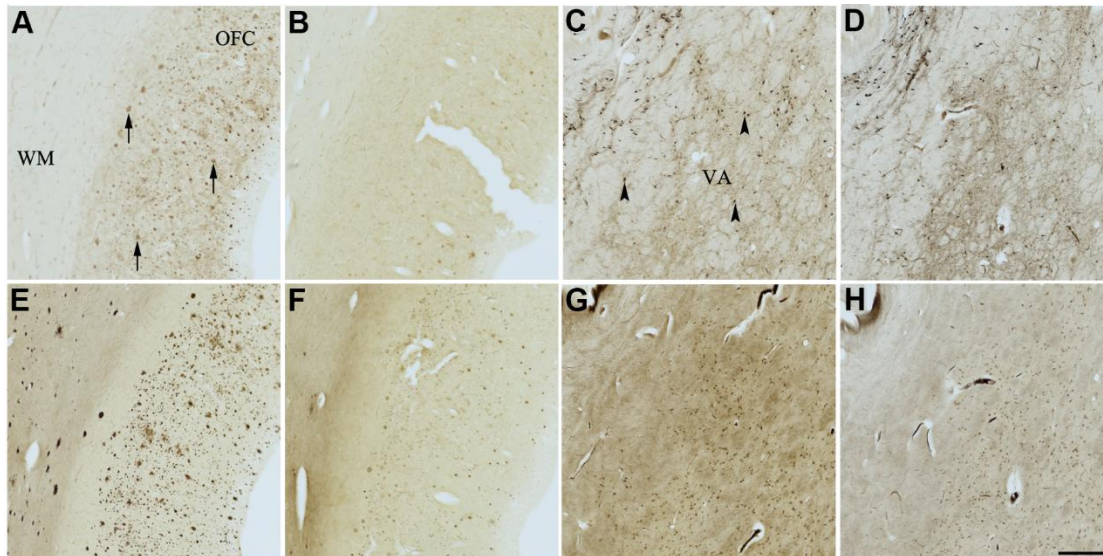


Figure 9. Effect of meclufenoxate hydrochloride (6) on histochemical staining of acetylcholinesterase (AChE) and butyrylcholinesterase (BChE). Representative photomicrographs of histochemical staining of AChE (A–D) and BChE (E–H). Staining at pH 6.8 demonstrates AChE- (A) and BChE (E)-associated plaques in the Alzheimer’s disease (AD) orbitofrontal cortex (arrows). Staining at pH 8.0 demonstrates AChE (C) and BChE (G) associated with normal neural structures in the AD thalamus (arrowheads showing neurons). Meclufenoxate hydrochloride (6) inhibits AChE (B) and, to a certain extent, BChE (F) associated with AD plaques but not AChE (D) and BChE (H) associated with normal neural elements. Note, for ease of reference, identical images of the positive control staining of AChE and BChE at pH 6.8 and 8.0 (A, C, E, G) were used herein and in Figures 4-8 (A, C, E, G) to help compare directly the effects of each senolytic or nootropic agent on the standard Karnovsky-Roots (KR) histochemical staining method. Abbreviations: OFC, orbitofrontal cortex; VA, ventroanterior thalamic nucleus; WM, white matter. Scale bar = 500 μ m.

Utilizing a blind docking approach [99], with five docking poses generated in each docking experiment and repeated in triplicate, compounds 1-6 localized to the same five main ChE sites (Figure 10C, 10D) identified using the Molecular Operating Environment (MOE) *Site Finder* feature. These five sites are denoted as follows: (I) enzyme active site gorge, (II) pocket behind ChE acyl loop, (III) pocket behind ChE catalytic glutamate and ϵ -helix, (IV) pocket behind key ChE

active site tryptophan (“Back Door”), and (V) other site located on the opposite side of the enzyme, away from the active site gorge. While blind docking experiments with compounds 1-6 did not show all five of these sites in each experiment, compound blind docking poses were distributed between these five ChE enzyme locations (Supplementary Table 1). These five binding pockets are displayed for each ChE crystal structure in Figure 10C, 10D.

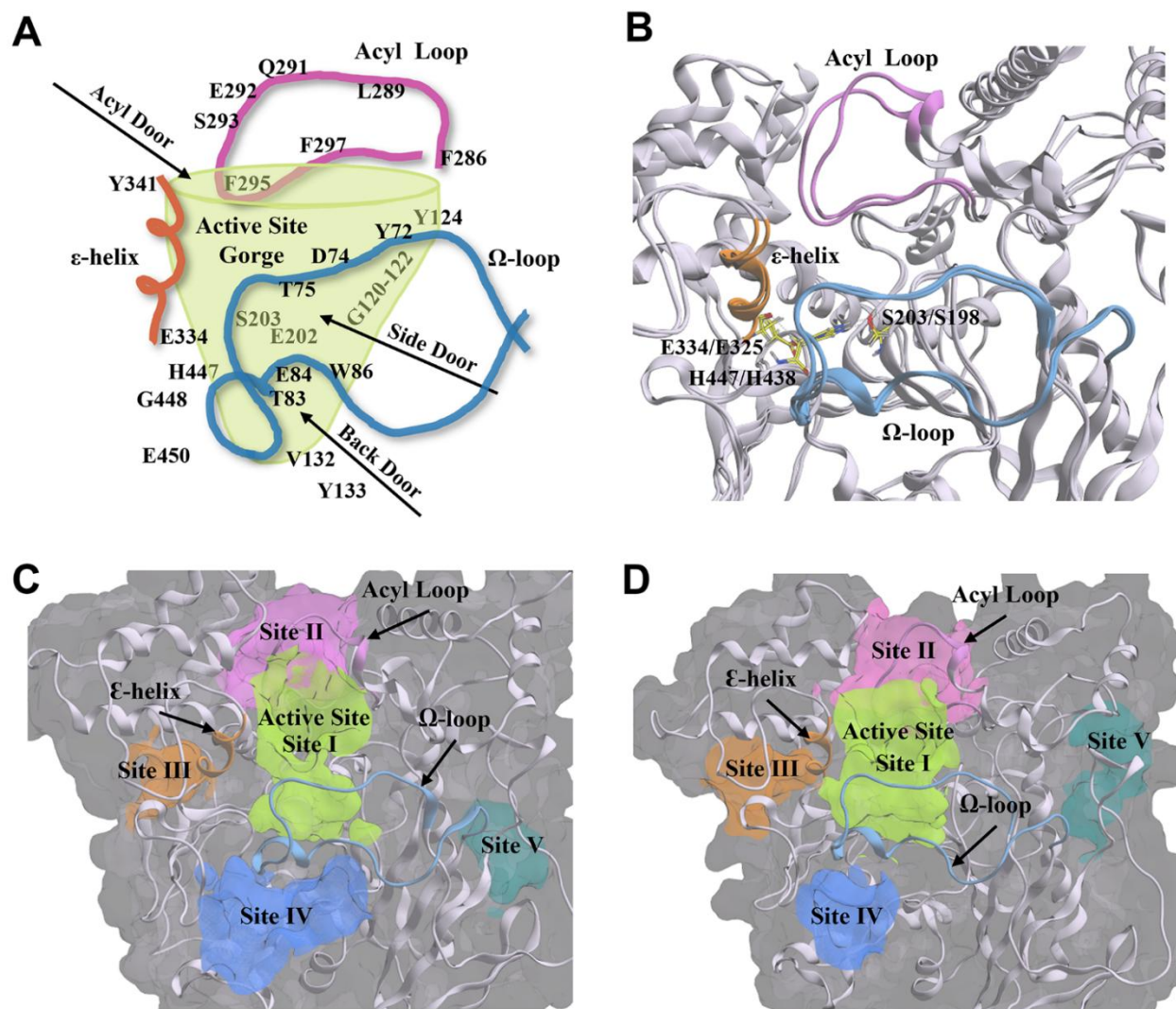


Figure 10. Structural components and amino acid residues that are essential for the catalytic activity of acetylcholinesterase (AChE) and butyrylcholinesterase (BChE). (A) 2D depiction of the entry/exit routes (“doors”) to the active site gorge of AChE. Amino acids are labelled and arranged according to their structural placement around the gorge, with those located on the opposite side to the viewing plane shown through the transparent green gorge wall. (B) AChE (PDB: 4M0E, 2.00 Å) [91] and BChE (BChE; PDB: 4TPK, 2.70 Å) [92] enzyme ribbon structures are overlaid to show structural conservation between the two enzymes. The catalytic triad residues are shown in yellow. (C, D) The five main compound binding site pockets (I-V) of AChE (C) and BChE (D) are identified as the enzyme active site gorge (lime green, I), pocket behind ChE acyl loop (pink, II), pocket behind ChE catalytic glutamate (orange, III), pocket behind ChE active site tryptophan (Back Door, blue, IV), and other binding pocket (teal, V). Structural features of AChE and BChE including the acyl loop (pink), Ω -loop (blue), and ϵ -helix (orange) are shown throughout each panel. Figures were generated using Microsoft PowerPoint for Microsoft 365 MSO (version 2409 build 18025.20104; Microsoft Corporation, Redmond, WA, USA) and Molecular Operating Environment 2022.02 (Chemical Computing Group ULC, Montreal, Quebec, Canada).

Senolytics 1 and 2 did not find the active site of either ChE enzyme in blind docking experiments (Supplementary Table 1). Compounds 3-6 localized to the active site of AChE, while compounds 3, 4, and 6 showed affinities for the active site of BChE (Supplementary Table 1). Compound 5 did not find the active site of BChE. Though compounds 3, 4, and 6 found the active site of both enzymes, only quercetin (4) with BChE and fisetin (3) with AChE showed predominant affinity for the active site gorge in blind docking poses (Supplementary Table 1). Compounds that did not find the active site (1, 2 for AChE; 1, 2, 5 for BChE) – or those that did not localize to the active site in the majority of blind docking poses (4, 5 for AChE; 3 for BChE) – showed affinity most frequently to one major site on each enzyme, site II for AChE and site III for BChE (Supplementary Table 1). Meclofenoxate hydrochloride (6) with both ChEs, and nintedanib (2) with AChE showed equal affinity (6/15 poses) for two sites. For compound 2, these sites were II and III of AChE (Supplementary Table 1), while for 6 these were sites I and III with BChE, and I and IV with AChE.

While it remains uncertain if the frequency of localization of blind docking poses to specific enzyme sites is indicative of true compound preference for that site, or simply a result of varying factors related to the blind modeling process [99–101], it is generally accepted that the failure of a compound to find the active site of an enzyme during blind docking experiments is predictive of the compound not interacting with that active site experimentally [99, 102–104]. Localization to sites beyond the active site gorge of an enzyme may indicate compound affinity for allosteric binding sites; thus, all compounds were assessed in site-directed docking experiments at all identified ChE sites. This resulted in some compounds having multiple calculated inhibition constants (K_i values) for different binding sites, which are summarized in the Supplementary Materials (Supplementary Table 2).

Predicted K_i values were generally within the same order of magnitude as experimentally determined K_i values but were highly variable depending on the enzyme site used for site-directed docking. For example, dasatinib (1) docked with BChE at site II had a sub-micromolar predicted K_i , while the dock directed to site III showed a predicted K_i that was almost identical to the experimental K_i value (Supplementary Table 2). Similarly, fisetin (3) and quercetin (4) found the active sites of both ChEs in blind docks but predicted K_i values at these sites were much lower than experimental values. However, the predicted K_i values at alternate sites for compounds 3 and 4 were closer to their experimental values (Table 1 and Supplementary

Table 2). For AChE, site II consistently showed K_i values closest to those determined experimentally (Table 1 and Supplementary Table 2). For BChE, there was more variability in alternate sites, but site III produced more accurate K_i values for several compounds (Table 1 and Supplementary Table 2).

Key amino acid interactions between compounds 1-6 and residues of each ChE were analyzed for the top site-directed docking pose at each identified site (I-V; Supplementary Table 3). Their interaction type, bond lengths, and residues' location on the enzyme were identified, with most being hydrogen bonding interactions. Overall, similar amino acid residue interactions were observed for compounds docked to the same site (I-V). Likewise, many of these residues were components of the acyl and Ω -loops, the ϵ -helix, or were residues of the five main regions of the ChE active site gorge (CAS, ABP, PAS, PCS, and OAH).

DISCUSSION

In normal aging, as well as in age-related diseases such as AD, there is abnormal accumulation of senescent cells in the brain [2, 3]. To address this, several senolytic agents have been used to mitigate cellular consequences of senescence [73, 74]. Both normal aging and AD are characterized by changes to the cholinergic system as reflected by reduction in the levels of acetylcholine, ChAT, nAChRs, mAChRs, and AChE [13, 31, 36], and an increase [32, 36, 38] or no change [37] to the levels of BChE. AChE and BChE are both associated with AD $A\beta$ plaques and tau neurofibrillary tangles [37, 39, 40]. The present work was undertaken to determine whether compounds used as senolytics or nootropics will inhibit ChEs, as these compounds display the clinical benefits of reducing senescent cells, SASP factors or lipofuscin and improving cognitive functions [73, 76–79, 81, 82]. It was reasoned that this knowledge might facilitate the development of next-generation ChEIs/senolytics to treat AD. We focused on evaluating the effects of senolytic and nootropic agents 1-6 on ChEs associated with $A\beta$ plaques and normal neural elements in human AD brain tissues, as well as evaluating the kinetic and *in silico* profiles of compounds to gain insights into their mechanisms of action.

Results from the experimental analyses undertaken showed that compounds 1-6 are ChE inhibitors, with most compounds showing inhibition of both ChEs using Ellman's method, with K_i values ranging from 7-110 μ M for AChE and 3-95 μ M for BChE. In enzyme kinetic studies, compounds showed mixed non-competitive inhibition, often indicative of allosteric binding [105], apart from fisetin (3) which was a competitive inhibitor

of AChE and an uncompetitive inhibitor of BChE. The potency of senolytic and nootropic agents 1-6 for ChEs is comparable to the known clinical ChE inhibitors that were previously investigated in *in vitro* and *in situ* studies [37]. For example, galantamine, a ChEI used in the symptomatic treatment of AD, showed inhibition of human AChE and BChE in the μM to sub- μM K_i range (0.52 μM for AChE, 2.09 μM for BChE) [37], indicating that senolytic and nootropic ChE inhibition is within pharmacological range to warrant future drug development of novel ChEIs based on senolytic and nootropic agents.

Questions about the mechanistic behavior of compounds 1-6 towards ChEs arose in relation to their behavior in histochemical studies. While it is relevant that compounds 1-6 inhibited ChEs in enzyme kinetic studies, it is known that the biochemical properties of AChE and BChE are altered when they are bound to AD pathology compared to when they are associated with normal neural structures [37, 44–46]. This is emphasized by the finding that compounds 1, 2, 5, and 6 selectively inhibit the histochemical staining of both ChEs associated with A β plaques but not those associated with normal neural structures. Further, it is of note that the AD drug galantamine inhibits ChE staining associated with both plaques and normal neural elements [37]. The selective, differential inhibition pattern of ChEs with some senolytics is a unique feature that will be desirable in the development of next-generation AD-modifying drugs that solely target pathology-associated ChEs. The selective inhibition of ChEs is consistent with a previous study that observed no effect on AChE activity in the brains of middle-aged and aged female wild-type mice when treated with a cocktail of compounds 1 and 3 [106]. As the KR histochemical method requires potassium ferricyanide and copper sulfate, we found that compounds 3 and 4 most likely chelated with these metals, precluding staining.

Molecular modeling studies were undertaken to determine potential compound binding interactions with ChEs and to help gain insight into their mechanisms of action. Overall, binding studies showed that all compounds have the propensity to bind to ChEs, with some of those being at the active site gorge and others at alternate enzyme binding sites that may represent allosteric binding pockets. Allosteric binding is of relevance as it remains to be determined which region(s) of AChE and BChE bind to A β plaques, and allosteric inhibitors may provide insight to this question. Previous studies have suggested that the PAS is the one of the key locations for A β binding with AChE [107–109] and BChE [110], and ChE association with A β can produce inhibitory or activating effects on ChE catalytic function [110, 111]. Given the observation that

plaque-bound ChEs but not normal neural-associated ChEs are inhibited by senolytic and nootropic agents in AD brain tissues, it is likely that the affinity of these compounds for ChE binding sites is increased when A β plaques are bound, either through binding to the active site gorge or allosteric sites. The major alternate binding sites on ChEs identified in molecular modeling studies (binding sites II and III; Figure 10) contain key amino acid residues and structural features that are already identified as important for substrate binding and catalysis. At site II this is the ABP and acyl loop [94, 112–116], while at site III this is the catalytic glutamate and Y332 (Y341 for BChE), which are important residues of the ϵ -helix [117–119]. Therefore, it is plausible that compound binding in or near these sites would alter catalytic activity or inhibit catalysis altogether. Generally, *in silico* docking studies showed that there are four main putative allosteric sites on ChEs that compounds 1-6 may be binding to produce inhibitory activity. As these sites are of relevance to both inhibition of activity and A β interactions [110, 111], they could be utilized as targets for the development of future ChEIs.

There are several limitations within the current study. This includes a broader, qualitative analysis of a relatively small sample size of sex- and age-matched human AD brain tissues, which precluded us from statistical analysis and examining the potential impact of sex, age and plaque load on the senolytic and nootropic inhibition of ChEs associated with AD pathology. The incidence of AD increases with age and this neurodegenerative disorder is more prevalent in females than males, not accounted for by longer life expectancy in females [120]. Studies have demonstrated that higher AD neuropathology is attendant with greater cognitive decline in females [121, 122]. Moreover, it has been shown that when BChE is knocked-out in the 5XFAD mouse model of amyloidosis, there is a significantly lower percentage of fibrillar A β plaques in cortical and subcortical regions than in the parent 5XFAD strain, an effect more pronounced in males [123, 124]. This finding makes the relationship of sex, age and ChE-related AD pathology to be a point of interest, particularly in the context of senolytic and nootropic inhibition. A larger sex and age-matched sample size would allow for identifying such differences, if any, and help facilitate development of disease-modifying senolytic or nootropic drugs that have sex-specific targets towards personalized medicine.

Previous studies in the senescence-accelerated prone 8 (SAMP8) mouse, a model of aging that recapitulates many of the cognitive and neuropathological characteristics of AD [125, 126], showed that AChE activity is unchanged while BChE activity is 2-fold

higher in the brain when compared to senescent-resistant control mice [22, 23]. AChE and BChE expression in the SAMP8 mouse brain was unchanged [22, 23] or not significantly changed [18] compared to control mice, with the exception of significantly increased BChE expression in the SAMP8 hippocampus [18]. The upregulation of BChE activity in the SAMP8 model is in accordance with similar findings in human AD brains [38, 41] and in AD mouse models of amyloidosis [123, 127]. The increase in activity but not expression of BChE in SAMP8 mice was primarily attributed to the increased abundance and phenotypic changes of neuroglia [22, 23], a major source of brain BChE [28, 128–132]. The upregulated proliferation and activation of neuroglia, as well as their sustained release of pro-inflammatory cytokines [22, 23], are characteristic hallmarks of SAMP8 mouse brains [133, 134], as well as human age-related senescent and AD brains [2].

Since the increasing accumulation of A β plaque deposits and senescent cells are capable of increasing inflammation through secretion of pro-inflammatory cytokines, the CAIP becomes important in modulating anti-inflammatory activities. In this pathway, there is increased inflammation with low levels of acetylcholine leading to the secretion of pro-inflammatory cytokines such as TNF- α , IL-1 β , and IL-6; however, in the presence of appropriate or increased levels of acetylcholine there is protection against inflammation via suppression of secreted pro-inflammatory cytokines [66, 67, 69, 72]. Due to the close, intrinsic relationship between BChE and neuroinflammation in age-related senescence and AD, there is justification for the use of BChE inhibitors [70, 71] to increase the availability of acetylcholine thereby modulating anti-inflammatory effects via the CAIP [61, 133, 135]. In this regard, all the senolytic and nootropic compounds evaluated herein are inhibitors of ChEs, particularly AChE and BChE that are bound to AD pathology. Although the anti-inflammatory effects of 1-6 could not be investigated in the post-mortem tissue model employed herein, it could be inferred that any possible anti-inflammatory effects of these compounds, produced through the inhibition of SASP factors, may be, in part, through modulation of the CAIP [71]. However, there may be other pathways that are also involved [136], including allosteric sites that could be involved in pre-empting association of these enzymes to AD pathology. Future work investigating the anti-inflammatory effect of compounds 1-6 on the CAIP or other pathways in *in vivo* or *in vitro* models will require further investigations.

In conclusion, the senolytic compounds evaluated herein may have beneficial effects on both aging and AD, at least in part, through modulation of AChE and

BChE associated with AD pathology. This work provides new opportunities for the development of the next generation of ChE inhibitors that specifically target AChE and BChE associated with AD pathology.

MATERIALS AND METHODS

Materials

Acetonitrile was purchased from Fisher Scientific (Ottawa, Ontario, Canada). Acetylthiocholine iodide (ATChI), butyrylthiocholine iodide (BTChI), BW 284c51, cobalt chloride, cupric sulfate, 3,3'-diaminobenzidine tetrahydrochloride (DAB), 5,5-dithio-bis-(2-nitrobenzoic acid) (DTNB), ethanol, ethopropazine, gelatin, potassium ferricyanide, recombinant human AChE, and sodium citrate were purchased from MilliporeSigma Canada Ltd. (Oakville, Ontario, Canada). Dasatinib, nintedanib (Bibfl120), fisentini, quercetin, and GW2580 were purchased from Adooq Biosciences (Irvine, CA, USA). Meclofenoxate hydrochloride was purchased from Combi-Blocks (San Diego, CA, USA). All chemicals were used as received from suppliers. BChE purified from human plasma was a gift from Dr. Oksana Lockridge (Eppley Institute, University of Nebraska Medical Center, Omaha, NE, USA). Enzyme kinetic experiments were performed using a VWR UV-1600PC spectrophotometer (VWR International LLC, Canada, Mississauga, Ontario, Canada) with M.Wave Professional software 1.0.20 (Azzota Scientific, DE, USA). All enzyme kinetic data were analyzed, and Lineweaver-Burk plots were generated for each enzyme kinetic experiment using Microsoft Excel for Microsoft 365 MSO (version 2409 build 18025.20104; Microsoft Corporation, Redmond, WA, USA). Plots were assembled into figures using Adobe Photoshop (CS 5, Version 12.0, San Diego, CA, USA).

Enzyme kinetic studies

Enzyme kinetic studies were performed as previously described [86], using Ellman's assay [137]. Briefly, in a quartz cuvette (1 cm pathlength), a 0.577 mM DTNB solution in 0.1 M potassium phosphate buffer (1.6 mL, pH 7.0) was combined at room temperature with either recombinant AChE (0.1 mL, 3.7 nM) in 0.005% aqueous gelatin or purified human serum BChE (0.1 mL, 5.85 nM) in 0.005% aqueous gelatin and mixed with a senolytic or nootropic compound (Figure 1) dissolved in 50% (v/v) aqueous acetonitrile (0.05 mL). Absorbance of the cuvette solution was measured at 412 nm and the instrument zeroed before initiation of the reaction with either the AChE substrate ATChI (0.05 mL, 166 μ M) or the BChE substrate BTChI (0.05 mL, 166 μ M), dissolved in water. Substrate concentrations were kept constant while the senolytic

concentrations varied (0-140 μM). Changes in absorbance ($\Delta A/\text{min}$), reflecting the rate of ATChI or BTChI hydrolysis with their respective enzymes, were recorded spectrophotometrically every 5 seconds for 1 minute.

As done previously [86], Lineweaver-Burk plots were generated for each senolytic and nootropic compound with the velocity (v) of each reaction determined using Beer's Law, where $v = (\Delta A/\text{min})/(\epsilon l)$, ϵ is the molar extinction coefficient for 5-thio-2-nitrobenzoic acid (TNB) ($13600 \text{ M}^{-1} \text{ cm}^{-1}$), and l is the cuvette pathlength (1 cm). Replotting the calculated slopes from each double reciprocal plot against senolytic and nootropic concentrations, gave the inhibitor constant (K_i , M) as the x-intercept. The mode of inhibition (competitive, non-competitive, mixed non-competitive, or uncompetitive) was also determined by analyzing the relational pattern of linear regressions for varying concentrations of the same senolytic or nootropic compound. Enzyme kinetic experiments were performed in triplicate and kinetic parameter values were averaged.

Brain tissues

Human orbitofrontal cortex and thalamic brain tissues were used to evaluate the effects of senolytic and nootropic compounds on brain ChE activity associated with A β plaques and normal neural elements (i.e. neurons, neuropil, and axons), respectively. Brain regions were chosen based on the known distribution of AChE and BChE associated with normal neural elements (i.e. thalamus) and A β plaques (i.e. orbitofrontal cortex), as done previously [41, 138]. Following approval from the Nova Scotia Health Research Ethics Board, post-mortem brain tissues from sex- and age-matched AD cases that fulfilled clinical [139] and neuropathological [140–142] criteria for AD were obtained from the Maritime Brain Tissue Bank, a Centralized Operation of Research Equipment and Supports (CORES) facility, Faculty of Medicine, Dalhousie University (Halifax, Nova Scotia, Canada). Demographic information related to the cases used in this study can be found in Table 2.

The brains were removed between 10-23 hr after death and bisected at the midline. One half of the brain was sent for neuropathological examination, and the other was used for histochemical studies. The tissues used for histochemical studies were cut into approximately 1 cm-thick coronal slabs and immersion fixed in 10% buffered formalin between 2.11-4 days. Slabs were cryoprotected in a graded series of sucrose (10-40%) in 0.1 M phosphate buffer (pH 7.4; PB) for a minimum of 48 hr per sucrose solution and stored in PB with 40% sucrose and 0.6% sodium azide. Orbitofrontal and thalamic regions were sub-sectioned from the slabs and

tissue blocks were cut into 50 μM -thick serial sections using a Leica SM2000R microtome with a Physitemp freezing stage and BFS-40MPA controller (Physitemp Instruments LLC, Clifton, NJ, USA). Tissue sections were stored at -20°C in in PB with 40% sucrose and 0.05% sodium azide until used.

Histochemical studies

Histochemical staining for AChE and BChE activity in brain tissues was done using a modified [42] Karnovsky-Roots (KR) method [143]. Tissue sections were first rinsed for 30 min in 0.1 M PB, followed by 30 min in 0.1 M PB with 15% hydrogen peroxide (H_2O_2) and then rinsed for 30 min with 0.1 M maleate buffer (MB; pH 6.8 or 7.4) prior to incubation in the KR solution. Sections stained for AChE were incubated in the KR solution for 1.75 hr, while sections stained for BChE were incubated for 2.5 hr. The KR staining solution contained 0.5 mM sodium citrate, 0.47 mM cupric sulfate, and 0.05 mM of potassium ferricyanide, a thioester ChE substrate and ChE inhibitor in MB at pH 6.8 to stain for ChEs associated with AD pathology or pH 8.0 to stain for ChEs associated with normal neural elements. For AChE staining, ATChI (0.4 mM) was used as the substrate and ethopropazine (0.06 mM) was used to inhibit BChE. For BChE staining, BTChI (0.8 mM) was used as the substrate and BW 284c51 (0.01 mM) was used to inhibit AChE. Following incubation in KR, sections were rinsed in distilled water (dH_2O) for 30 min, incubated in a 0.1% cobalt chloride solution in dH_2O for 10 min, and rinsed again in dH_2O for 30 min. Sections were incubated in 1.39 mM 3,3'-diaminobenzidine tetrahydrochloride (DAB) in PB (pH 7.4) for 5 min and then developed using 50 μL of 0.3% H_2O_2 per mL of DAB solution. The reaction was stopped by a 30 min rinse in 0.01 M acetate buffer (pH 3.3). Stained sections were mounted on glass slides, cover-slipped and examined with brightfield microscopy.

To evaluate the interactions of senolytic and nootropic compounds with ChEs in brain tissues, the above histochemical technique was used with minor variations to the KR incubation [88]. Senolytic and nootropic compounds were dissolved in 50% aqueous acetonitrile to make a stock solution. The same volume of each compound was added individually to the KR solution; 0.25 mM dasatinib (1); 0.27 mM nintedanib (2); 1.3 mM fisetin (3); 1.3 mM quercetin (4); 0.4 mM GW2580 (5); and 1.3 mM meclufenoxate hydrochloride (6). Following incubation for AChE (1.75 hr) and BChE (2.5 hr) in the KR solution, staining was completed as described above.

To ensure specificity of staining and that changes in staining were due to the presence of compounds 1-6, control experiments were conducted. Positive controls

included staining for BChE and AChE activity at pH 6.8 and pH 8.0 without any additions. Negative controls were utilized to validate staining specificity of BChE and AChE at pH 6.8 and pH 8.0, where the substrates (BTChI and ATChI, respectively) were omitted, as previously described [88]. When the substrates were omitted, no BChE or AChE staining was observed. An additional control experiment was used to test the effect of the carrier solvent for compounds 1-6 (50% aqueous acetonitrile) on KR staining. Briefly, 50% aqueous acetonitrile was added to the KR solution, without any senolytic or nootropic compound, while maintaining the same volume as the compound additives. When 50% aqueous acetonitrile was used in KR staining, background staining intensity increased for AChE pH 6.8, while both AChE and BChE pH 6.8 plaques showed some reduction in overall staining. The extent of reduction by carrier solvent did not preclude evaluation of the inhibitory effects of compounds 1-6 on ChE histochemical staining. There were no observed effects on normal neural elements at pH 8.0.

A qualitative method was used to evaluate the effect of senolytic and nootropic compounds on ChE histochemical staining, as done previously [88]. Inhibition of staining intensity was categorized as follows: No reduction (-), slight (x), moderate (xx), or strong (xxx). Tissue sections were analyzed using brightfield microscopy on an Olympus BX50F microscope (Olympus Optical Co., Ltd., Tokyo, Japan). Photomicrographs of the stained tissue sections were taken using a Zeiss Axio Scan.Z1 slide scanner with Zen 3.1 Blue Edition software (Carl Zeiss Canada Ltd., Toronto, Ontario, Canada). Figures were assembled using Adobe Photoshop (CS 5, Version 12.0, San Diego, CA, USA). The brightness of each individual image was adjusted to ensure backgrounds matched for analysis.

Molecular docking studies

To determine predicted binding sites for the senolytic and nootropic agents with human AChE and BChE, compounds were docked using a reversible inhibitor docking procedure with Molecular Operating Environment (MOE) software 2022.02 (Chemical Computing Group, Montreal, Canada), as previously described [144, 145]. This docking procedure consisted of a blind docking phase, in which all compounds were allowed to dock anywhere on the enzyme, and a site-directed docking phase, in which compounds were directed to dock to their respective enzyme active site or other sites identified through blind docking. Blind docks were conducted to determine whether a compound was likely to find the active site of a given enzyme or if other enzyme locations, such as allosteric

sites, were also favorable for compound binding. Site-directed docks were conducted to determine possible key interactions between the compound and enzyme residues and to predict inhibition constants (K_i values).

Crystal structures for human AChE (Protein Databank code (PDB): 4MOE, 2.00 Å resolution) [91] and BChE (PDB: 4TPK, 2.70 Å) [92] were obtained from the Protein Databank [146] and were selected based on resolution and co-crystallization properties deemed appropriate for molecular docking [100]. Crystal structures were prepared for molecular docking as previously described [144] with all water molecules removed. Enzyme sites from blind docks were analyzed to identify locations for subsequent site-directed docks. The binding energies of the top five returned site-directed dock poses, key amino acid interactions, and bond lengths were identified and measured within MOE. Docks were completed in triplicate and their binding energies were converted to predicted K_i values using Gibb's free energy equation and averaged, as done previously [147].

Abbreviations

A β : amyloid- β ; ABP: acyl binding pocket; AChE: acetylcholinesterase; AD: Alzheimer's disease; ATChI: acetylthiocholine iodide; BChE: butyrylcholinesterase; Bibfl120: nintedanib; BTChI: butyrylthiocholine iodide; CAIP: cholinergic anti-inflammatory pathway; CAS: catalytic active site; ChAT: choline acetyltransferase; ChE: cholinesterase; ChEI: cholinesterase inhibitor; DAB: 3,3'-diaminobenzidine tetrahydrochloride; dH₂O: distilled water; DTNB: 5,5-dithio-bis-(2-nitrobenzoic acid); K_i : inhibition constant; H₂O₂: hydrogen peroxide; IL-1 β : interleukin 1 β ; IL-6: interleukin 6; KR: Karnovsky-Roots; mAChR: muscarinic acetylcholine receptor; MOE: Molecular Operating Environment; nAChR: nicotinic acetylcholine receptor; OAH: oxyanion hole; PAS: peripheral anionic site; PB: phosphate buffer; PCS: π -cationic site; PDB: Protein Databank; SAMP8: senescence-accelerated prone 8 mouse; SASP: senescence-associated secretory phenotype; TNB: 5-thio-2-nitrobenzoic acid; TNF α : tumor necrosis factor α .

AUTHOR CONTRIBUTIONS

Sultan Darvesh: Conceptualization, Data curation, Formal analysis, Funding acquisition, Project administration, Resources, Supervision, Validation, Writing – original draft, Writing – review and editing; Meghan K. Cash: Writing – original draft, Writing – review and editing; Katrina Forrestall: Data curation, Formal analysis, Investigation, Validation, Visualization, Writing - original draft, Writing – review and editing; Hillary Maillet: Data curation, Formal analysis,

Investigation, Validation, Visualization, Writing - original draft, Writing – review and editing; Dane Sands: Formal analysis, Investigation, Visualization, Writing – review and editing.

ACKNOWLEDGMENTS

We would like to thank Andrew Davis for their technical assistance.

CONFLICTS OF INTEREST

Sultan Darvesh is a scientific co-founder and stockholder in the Treventis Corporation, a biotech company focused on the development of diagnostic and therapeutic agents for Alzheimer's disease. Sultan Darvesh is listed as an inventor on patents assigned to Treventis Corporation. Also, Sultan Darvesh is an Associate Editor of Current Alzheimer Research. All other authors do not have financial disclosures or conflicts of interest to declare.

ETHICAL STATEMENT AND CONSENT

All post-mortem tissues used in this research were obtained from the Maritime Brain Tissue Bank, Halifax, Canada, in accordance with their tissue request guidelines and with approval from the Nova Scotia Health Research Ethics Board (REB File #: 1020654). The Maritime Brain Tissue Bank collects donated human brain tissues for research purposes with consent of the next-of-kin and attending physicians. Each donation (brain and related information) is de-identified by Maritime Brain Tissue Bank staff with unique assigned number to ensure the anonymity and confidentiality of its donors. The brain tissues provided by The Maritime Brain Tissue Bank for our research have already received the necessary consent for use.

FUNDING

This work was supported in part by the Canadian Institutes of Health Research (PJT – 153319), the Dalhousie Medical Research Foundation (DMRF Chemists, DMRF Clare Durland Fund in Alzheimer's Disease Research; DMRF Research Grant – Robert and Barbara Pickett; DMRF Gillian's Hope for MS Research Fund), and the Dalhousie University Endowed Irene MacDonald Sobey Endowed Chair in Curative Approaches to Alzheimer's Disease.

REFERENCES

1. Hayflick L, Moorhead PS. The serial cultivation of human diploid cell strains. *Exp Cell Res.* 1961;

25:585–621.

[https://doi.org/10.1016/0014-4827\(61\)90192-6](https://doi.org/10.1016/0014-4827(61)90192-6)

PMID:[13905658](https://pubmed.ncbi.nlm.nih.gov/13905658/)

2. Saez-Atienzar S, Masliah E. Cellular senescence and Alzheimer disease: the egg and the chicken scenario. *Nat Rev Neurosci.* 2020; 21:433–44.
<https://doi.org/10.1038/s41583-020-0325-z>
PMID:[32601397](https://pubmed.ncbi.nlm.nih.gov/32601397/)
3. Holloway K, Neherin K, Dam KU, Zhang H. Cellular senescence and neurodegeneration. *Hum Genet.* 2023; 142:1247–62.
<https://doi.org/10.1007/s00439-023-02565-x>
PMID:[37115318](https://pubmed.ncbi.nlm.nih.gov/37115318/)
4. Engeland K. Cell cycle regulation: p53-p21-RB signaling. *Cell Death Differ.* 2022; 29:946–60.
<https://doi.org/10.1038/s41418-022-00988-z>
PMID:[35361964](https://pubmed.ncbi.nlm.nih.gov/35361964/)
5. Safwan-Zaiter H, Wagner N, Wagner KD. P16INK4A-More Than a Senescence Marker. *Life (Basel).* 2022; 12:1332.
<https://doi.org/10.3390/life12091332> PMID:[36143369](https://pubmed.ncbi.nlm.nih.gov/36143369/)
6. Dimri GP, Lee X, Basile G, Acosta M, Scott G, Roskelley C, Medrano EE, Linskens M, Rubelj I, Pereira-Smith O. A biomarker that identifies senescent human cells in culture and in aging skin *in vivo*. *Proc Natl Acad Sci USA.* 1995; 92:9363–7.
<https://doi.org/10.1073/pnas.92.20.9363>
PMID:[7568133](https://pubmed.ncbi.nlm.nih.gov/7568133/)
7. Georgakopoulou EA, Tsimaratou K, Evangelou K, Fernandez Marcos PJ, Zoumpourlis V, Trougakos IP, Kletsas D, Bartek J, Serrano M, Gorgoulis VG. Specific lipofuscin staining as a novel biomarker to detect replicative and stress-induced senescence. A method applicable in cryo-preserved and archival tissues. *Aging (Albany NY).* 2013; 5:37–50.
<https://doi.org/10.18632/aging.100527>
PMID:[23449538](https://pubmed.ncbi.nlm.nih.gov/23449538/)
8. Baker DJ, Petersen RC. Cellular senescence in brain aging and neurodegenerative diseases: evidence and perspectives. *J Clin Invest.* 2018; 128:1208–16.
<https://doi.org/10.1172/JCI95145> PMID:[29457783](https://pubmed.ncbi.nlm.nih.gov/29457783/)
9. Di Micco R, Krizhanovsky V, Baker D, d'Adda di Fagagna F. Cellular senescence in ageing: from mechanisms to therapeutic opportunities. *Nat Rev Mol Cell Biol.* 2021; 22:75–95.
<https://doi.org/10.1038/s41580-020-00314-w>
PMID:[33328614](https://pubmed.ncbi.nlm.nih.gov/33328614/)
10. Jurk D, Wang C, Miwa S, Maddick M, Korolchuk V, Tsolou A, Gonos ES, Thrasivoulou C, Saffrey MJ, Cameron K, von Zglinicki T. Postmitotic neurons develop a p21-dependent senescence-like phenotype

- driven by a DNA damage response. *Aging Cell*. 2012; 11:996–1004.
<https://doi.org/10.1111/j.1474-9726.2012.00870.x>
PMID:22882466
11. Gallagher M, Colombo PJ. Ageing: the cholinergic hypothesis of cognitive decline. *Curr Opin Neurobiol*. 1995; 5:161–8.
[https://doi.org/10.1016/0959-4388\(95\)80022-0](https://doi.org/10.1016/0959-4388(95)80022-0)
PMID:7620303
 12. Orlando IF, Shine JM, Robbins TW, Rowe JB, O’Callaghan C. Noradrenergic and cholinergic systems take centre stage in neuropsychiatric diseases of ageing. *Neurosci Biobehav Rev*. 2023; 149:105167.
<https://doi.org/10.1016/j.neubiorev.2023.105167>
PMID:37054802
 13. Schliebs R, Arendt T. The cholinergic system in aging and neuronal degeneration. *Behav Brain Res*. 2011; 221:555–63.
<https://doi.org/10.1016/j.bbr.2010.11.058>
PMID:21145918
 14. Gibson GE, Peterson C, Jenden DJ. Brain acetylcholine synthesis declines with senescence. *Science*. 1981; 213:674–6.
<https://doi.org/10.1126/science.7256270>
PMID:7256270
 15. Ikegami S, Shumiya S, Kawamura H. Age-related changes in radial-arm maze learning and basal forebrain cholinergic systems in senescence accelerated mice (SAM). *Behav Brain Res*. 1992; 51:15–22.
[https://doi.org/10.1016/s0166-4328\(05\)80307-9](https://doi.org/10.1016/s0166-4328(05)80307-9)
PMID:1482543
 16. Perry EK, Piggott MA, Court JA, Johnson M, Perry RH. Transmitters in the developing and senescent human brain. *Ann N Y Acad Sci*. 1993; 695:69–72.
<https://doi.org/10.1111/j.1749-6632.1993.tb23030.x>
PMID:7902056
 17. Liu D, Hsueh SC, Tweedie D, Price N, Glotfelty E, Lecca D, Telljohann R, deCabo R, Hoffer BJ, Greig NH. Chronic inflammation with microglia senescence at basal forebrain: impact on cholinergic deficit in Alzheimer’s brain haemodynamics. *Brain Commun*. 2024; 6:fcae204.
<https://doi.org/10.1093/braincomms/fcae204>
PMID:38978722
 18. Reale M, Costantini E, Aielli L, Di Giuseppe F, Angelucci S, Kamal MA, Greig NH. Proteomic Signature and mRNA Expression in Hippocampus of SAMP8 and SAMR1 Mice during Aging. *Int J Mol Sci*. 2022; 23:15097.
<https://doi.org/10.3390/ijms232315097>
PMID:36499421
 19. Vijayan VK. Cholinergic enzymes in the cerebellum and the hippocampus of the senescent mouse. *Exp Gerontol*. 1977; 12:7–11.
[https://doi.org/10.1016/0531-5565\(77\)90026-2](https://doi.org/10.1016/0531-5565(77)90026-2)
PMID:885175
 20. Kabuto H, Yokoi I, Mori A, Murakami M, Sawada S. Neurochemical changes related to ageing in the senescence-accelerated mouse brain and the effect of chronic administration of nimodipine. *Mech Ageing Dev*. 1995; 80:1–9.
[https://doi.org/10.1016/0047-6374\(94\)01542-t](https://doi.org/10.1016/0047-6374(94)01542-t)
PMID:7564556
 21. Nitta A, Naruhashi K, Umemura M, Hasegawa T, Furukawa S, Sekiguchi F, Ishibashi K, Nabeshima T. Age-related changes in learning and memory and cholinergic neuronal function in senescence accelerated mice (SAM). *Behav Brain Res*. 1995; 72:49–55.
[https://doi.org/10.1016/0166-4328\(96\)00040-x](https://doi.org/10.1016/0166-4328(96)00040-x)
PMID:8788856
 22. Fernández-Gómez FJ, Muñoz-Delgado E, Montenegro MF, Campoy FJ, Vidal CJ, Jordán J. The level of butyrylcholinesterase activity increases and the content of the mRNA remains unaffected in brain of senescence-accelerated mouse SAMP8. *Chem Biol Interact*. 2008; 175:332–5.
<https://doi.org/10.1016/j.cbi.2008.05.010>
PMID:18571151
 23. Fernández-Gómez FJ, Muñoz-Delgado E, Montenegro MF, Campoy FJ, Vidal CJ, Jordán J. Cholinesterase activity in brain of senescence-accelerated-resistant mouse SAMR1 and its variation in brain of senescence-accelerated-prone mouse SAMP8. *J Neurosci Res*. 2010; 88:155–66.
<https://doi.org/10.1002/jnr.22177>
PMID:19610099
 24. Darvesh S, Hopkins DA, Geula C. Neurobiology of butyrylcholinesterase. *Nat Rev Neurosci*. 2003; 4:131–8.
<https://doi.org/10.1038/nrn1035>
PMID:12563284
 25. Lockridge O. Review of human butyrylcholinesterase structure, function, genetic variants, history of use in the clinic, and potential therapeutic uses. *Pharmacol Ther*. 2015; 148:34–46.
<https://doi.org/10.1016/j.pharmthera.2014.11.011>
PMID:25448037
 26. Darvesh S, Grantham DL, Hopkins DA. Distribution of butyrylcholinesterase in the human amygdala and hippocampal formation. *J Comp Neurol*. 1998; 393:374–90.
PMID:9548556
 27. Friede RL. A comparative histochemical mapping of the distribution of butyryl cholinesterase in the brains of

- four species of mammals, including man. *Acta Anat* (Basel). 1967; 66:161–77.
<https://doi.org/10.1159/000142920>
PMID:[4964503](https://pubmed.ncbi.nlm.nih.gov/4964503/)
28. Silver A. *The Biology of Cholinesterases*. (Amsterdam, Netherlands: North-Holland Publishing Company). 1974.
29. Massoulié J, Sussman J, Bon S, Silman I. Structure and functions of acetylcholinesterase and butyrylcholinesterase. *Prog Brain Res*. 1993; 98:139–46.
[https://doi.org/10.1016/s0079-6123\(08\)62391-2](https://doi.org/10.1016/s0079-6123(08)62391-2)
PMID:[8248501](https://pubmed.ncbi.nlm.nih.gov/8248501/)
30. Villeda-González JD, Gómez-Olivares JL, Baiza-Gutman LA. New paradigms in the study of the cholinergic system and metabolic diseases: Acetyl-and-butryrylcholinesterase. *J Cell Physiol*. 2024; 239:e31274.
<https://doi.org/10.1002/jcp.31274>
PMID:[38605655](https://pubmed.ncbi.nlm.nih.gov/38605655/)
31. Pepeu G, Giovannelli L. The central cholinergic system during aging. *Prog Brain Res*. 1994; 100:67–71.
[https://doi.org/10.1016/s0079-6123\(08\)60770-0](https://doi.org/10.1016/s0079-6123(08)60770-0)
PMID:[7938536](https://pubmed.ncbi.nlm.nih.gov/7938536/)
32. Perry EK. The cholinergic system in old age and Alzheimer's disease. *Age Ageing*. 1980; 9:1–8.
<https://doi.org/10.1093/ageing/9.1.1> PMID:[7361631](https://pubmed.ncbi.nlm.nih.gov/7361631/)
33. Chaves-Coira I, García-Magro N, Zegarra-Valdivia J, Torres-Alemán I, Núñez Á. Cognitive Deficits in Aging Related to Changes in Basal Forebrain Neuronal Activity. *Cells*. 2023; 12:1477.
<https://doi.org/10.3390/cells12111477>
PMID:[37296598](https://pubmed.ncbi.nlm.nih.gov/37296598/)
34. Bartus RT, Dean RL 3rd, Beer B, Lippa AS. The cholinergic hypothesis of geriatric memory dysfunction. *Science*. 1982; 217:408–14.
<https://doi.org/10.1126/science.7046051>
PMID:[7046051](https://pubmed.ncbi.nlm.nih.gov/7046051/)
35. Coyle JT, Price DL, DeLong MR. Alzheimer's disease: a disorder of cortical cholinergic innervation. *Science*. 1983; 219:1184–90.
<https://doi.org/10.1126/science.6338589>
PMID:[6338589](https://pubmed.ncbi.nlm.nih.gov/6338589/)
36. Perry EK, Perry RH, Blessed G, Tomlinson BE. Changes in brain cholinesterases in senile dementia of Alzheimer type. *Neuropathol Appl Neurobiol*. 1978; 4:273–7.
<https://doi.org/10.1111/j.1365-2990.1978.tb00545.x>
PMID:[703927](https://pubmed.ncbi.nlm.nih.gov/703927/)
37. Darvesh S, Reid GA, Martin E. Biochemical and histochemical comparison of cholinesterases in normal and Alzheimer brain tissues. *Curr Alzheimer Res*. 2010; 7:386–400.
<https://doi.org/10.2174/156720510791383868>
PMID:[19939227](https://pubmed.ncbi.nlm.nih.gov/19939227/)
38. Atack JR, Perry EK, Bonham JR, Candy JM, Perry RH. Molecular forms of butyrylcholinesterase in the human neocortex during development and degeneration of the cortical cholinergic system. *J Neurochem*. 1987; 48:1687–92.
<https://doi.org/10.1111/j.1471-4159.1987.tb05724.x>
PMID:[3572398](https://pubmed.ncbi.nlm.nih.gov/3572398/)
39. Mesulam MM, Geula C. Butyrylcholinesterase reactivity differentiates the amyloid plaques of aging from those of dementia. *Ann Neurol*. 1994; 36:722–7.
<https://doi.org/10.1002/ana.410360506>
PMID:[7979218](https://pubmed.ncbi.nlm.nih.gov/7979218/)
40. Geula C, Mesulam MM. Cholinesterases and the pathology of Alzheimer disease. *Alzheimer Dis Assoc Disord*. 1995; 9:23–8.
<https://doi.org/10.1097/00002093-199501002-00005>
PMID:[8534419](https://pubmed.ncbi.nlm.nih.gov/8534419/)
41. Macdonald IR, Maxwell SP, Reid GA, Cash MK, DeBay DR, Darvesh S. Quantification of Butyrylcholinesterase Activity as a Sensitive and Specific Biomarker of Alzheimer's Disease. *J Alzheimers Dis*. 2017; 58:491–505.
<https://doi.org/10.3233/JAD-170164> PMID:[28453492](https://pubmed.ncbi.nlm.nih.gov/28453492/)
42. Maxwell SP, Cash MK, Darvesh S. Neuropathology and cholinesterase expression in the brains of octogenarians and older. *Chem Biol Interact*. 2022; 364:110065.
<https://doi.org/10.1016/j.cbi.2022.110065>
PMID:[35872043](https://pubmed.ncbi.nlm.nih.gov/35872043/)
43. Maxwell SPL. Clinicopathological Correlates in Tauopathy and Aging. *Medical Neuroscience*. (Halifax, Canada: Dalhousie University). 2022; 1–197.
44. Geula C, Mesulam M. Special properties of cholinesterases in the cerebral cortex of Alzheimer's disease. *Brain Res*. 1989; 498:185–9.
[https://doi.org/10.1016/0006-8993\(89\)90419-8](https://doi.org/10.1016/0006-8993(89)90419-8)
PMID:[2790472](https://pubmed.ncbi.nlm.nih.gov/2790472/)
45. Reid GA, Darvesh S. Interaction of Exogenous Butyrylcholinesterase with β -Amyloid Plaques in 5XFAD/Butyrylcholinesterase-Knockout Mouse Brain. *Curr Alzheimer Res*. 2021; 18:470–81.
<https://doi.org/10.2174/1567205018666210827122704> PMID:[34455970](https://pubmed.ncbi.nlm.nih.gov/34455970/)
46. Reid GA, Darvesh S. Interaction of exogenous acetylcholinesterase and butyrylcholinesterase with amyloid- β plaques in human brain tissue. *Chem Biol Interact*. 2024; 395:111012.
<https://doi.org/10.1016/j.cbi.2024.111012>
PMID:[38648920](https://pubmed.ncbi.nlm.nih.gov/38648920/)

47. Wright CI, Geula C, Mesulam MM. Neurological cholinesterases in the normal brain and in Alzheimer's disease: relationship to plaques, tangles, and patterns of selective vulnerability. *Ann Neurol*. 1993; 34:373–84.
<https://doi.org/10.1002/ana.410340312>
PMID:[8363355](https://pubmed.ncbi.nlm.nih.gov/8363355/)
48. Gok M, Cicek C, Bodur E. Butyrylcholinesterase in lipid metabolism: A new outlook. *J Neurochem*. 2024; 168:381–5.
<https://doi.org/10.1111/jnc.15833>
PMID:[37129444](https://pubmed.ncbi.nlm.nih.gov/37129444/)
49. Jasiński J, Szczoczarz A, Cysewski D, Lewandowski K, Skowron P, Waleron K, Wasąg B. Butyrylcholinesterase-Protein Interactions in Human Serum. *Int J Mol Sci*. 2021; 22:10662.
<https://doi.org/10.3390/ijms221910662>
PMID:[34639003](https://pubmed.ncbi.nlm.nih.gov/34639003/)
50. Paraoanu LE, Steinert G, Klaczinski J, Becker-Röck M, Bytyqi A, Layer PG. On functions of cholinesterases during embryonic development. *J Mol Neurosci*. 2006; 30:201–4.
<https://doi.org/10.1385/JMN:30:1:201>
PMID:[17192676](https://pubmed.ncbi.nlm.nih.gov/17192676/)
51. Vidal CJ. Expression of cholinesterases in brain and non-brain tumours. *Chem Biol Interact*. 2005; 157–158:227–32.
<https://doi.org/10.1016/j.cbi.2005.10.035>
PMID:[16256970](https://pubmed.ncbi.nlm.nih.gov/16256970/)
52. Johnson G, Moore SW. Cholinesterases modulate cell adhesion in human neuroblastoma cells *in vitro*. *Int J Dev Neurosci*. 2000; 18:781–90.
[https://doi.org/10.1016/s0736-5748\(00\)00049-6](https://doi.org/10.1016/s0736-5748(00)00049-6)
PMID:[11154847](https://pubmed.ncbi.nlm.nih.gov/11154847/)
53. Comoletti D, Trobiani L, Chatonnet A, Bourne Y, Marchot P. Comparative mapping of selected structural determinants on the extracellular domains of cholinesterase-like cell-adhesion molecules. *Neuropharmacology*. 2021; 184:108381.
<https://doi.org/10.1016/j.neuropharm.2020.108381>
PMID:[33166544](https://pubmed.ncbi.nlm.nih.gov/33166544/)
54. Barbosa M, Rios O, Velásquez M, Villalobos J, Ehrmanns J. Acetylcholinesterase and butyrylcholinesterase histochemical activities and tumor cell growth in several brain tumors. *Surg Neurol*. 2001; 55:106–12.
[https://doi.org/10.1016/s0090-3019\(01\)00351-2](https://doi.org/10.1016/s0090-3019(01)00351-2)
PMID:[11301094](https://pubmed.ncbi.nlm.nih.gov/11301094/)
55. Baranowska-Kortylewicz J, Kortylewicz ZP, McIntyre EM, Sharp JG, Coulter DW. Multifarious Functions of Butyrylcholinesterase in Neuroblastoma: Impact of BCHE Deletion on the Neuroblastoma Growth *In Vitro* and *In Vivo*. *J Pediatr Hematol Oncol*. 2022; 44:293–304.
<https://doi.org/10.1097/MPH.0000000000002285>
PMID:[34486544](https://pubmed.ncbi.nlm.nih.gov/34486544/)
56. Mack A, Robitzki A. The key role of butyrylcholinesterase during neurogenesis and neural disorders: an antisense-5'butyrylcholinesterase-DNA study. *Prog Neurobiol*. 2000; 60:607–28.
[https://doi.org/10.1016/s0301-0082\(99\)00047-7](https://doi.org/10.1016/s0301-0082(99)00047-7)
PMID:[10739090](https://pubmed.ncbi.nlm.nih.gov/10739090/)
57. Carneiro BA, El-Deiry WS. Targeting apoptosis in cancer therapy. *Nat Rev Clin Oncol*. 2020; 17:395–417.
<https://doi.org/10.1038/s41571-020-0341-y>
PMID:[32203277](https://pubmed.ncbi.nlm.nih.gov/32203277/)
58. Blagosklonny MV. Anti-aging: senolytics or gerostatics (unconventional view). *Oncotarget*. 2021; 12:1821–35.
<https://doi.org/10.18632/oncotarget.28049>
PMID:[34504654](https://pubmed.ncbi.nlm.nih.gov/34504654/)
59. Skrzypek A, Karpińska M, Juszcak M, Grabarska A, Wietrzyk J, Krajewska-Kulak E, Studziński M, Paszko T, Matysiak J. Cholinesterases Inhibition, Anticancer and Antioxidant Activity of Novel Benzoxazole and Naphthoxazole Analogs. *Molecules*. 2022; 27:8511.
<https://doi.org/10.3390/molecules27238511>
PMID:[36500605](https://pubmed.ncbi.nlm.nih.gov/36500605/)
60. Katalinić M, Rusak G, Domaćinović Barović J, Sinko G, Jelić D, Antolović R, Kovarik Z. Structural aspects of flavonoids as inhibitors of human butyrylcholinesterase. *Eur J Med Chem*. 2010; 45:186–92.
<https://doi.org/10.1016/j.ejmech.2009.09.041>
PMID:[19879672](https://pubmed.ncbi.nlm.nih.gov/19879672/)
61. Macdonald IR, Rockwood K, Martin E, Darvesh S. Cholinesterase inhibition in Alzheimer's disease: is specificity the answer? *J Alzheimers Dis*. 2014; 42:379–84.
<https://doi.org/10.3233/JAD-140219> PMID:[24898642](https://pubmed.ncbi.nlm.nih.gov/24898642/)
62. Birks J. Cholinesterase inhibitors for Alzheimer's disease. *Cochrane Database Syst Rev*. 2006; 2006:CD005593.
<https://doi.org/10.1002/14651858.CD005593>
PMID:[16437532](https://pubmed.ncbi.nlm.nih.gov/16437532/)
63. Arias E, Gallego-Sandín S, Villarroya M, García AG, López MG. Unequal neuroprotection afforded by the acetylcholinesterase inhibitors galantamine, donepezil, and rivastigmine in SH-SY5Y neuroblastoma cells: role of nicotinic receptors. *J Pharmacol Exp Ther*. 2005; 315:1346–53.
<https://doi.org/10.1124/jpet.105.090365>
PMID:[16144975](https://pubmed.ncbi.nlm.nih.gov/16144975/)
64. Gupta P, Tiwari S, Singh A, Pal A, Mishra A, Singh S. Rivastigmine attenuates the Alzheimer's disease related protein degradation and apoptotic neuronal

- death signalling. *Biochem J.* 2021; 478:1435–51.
<https://doi.org/10.1042/BCJ20200754>
PMID:[33660768](https://pubmed.ncbi.nlm.nih.gov/33660768/)
65. Reale M, Iarlori C, Gambi F, Lucci I, Salvatore M, Gambi D. Acetylcholinesterase inhibitors effects on oncostatin-M, interleukin-1 beta and interleukin-6 release from lymphocytes of Alzheimer's disease patients. *Exp Gerontol.* 2005; 40:165–71.
<https://doi.org/10.1016/j.exger.2004.12.003>
PMID:[15763393](https://pubmed.ncbi.nlm.nih.gov/15763393/)
66. Pavlov VA, Parrish WR, Rosas-Ballina M, Ochani M, Puerta M, Ochani K, Chavan S, Al-Abed Y, Tracey KJ. Brain acetylcholinesterase activity controls systemic cytokine levels through the cholinergic anti-inflammatory pathway. *Brain Behav Immun.* 2009; 23:41–45.
<https://doi.org/10.1016/j.bbi.2008.06.011>
PMID:[18639629](https://pubmed.ncbi.nlm.nih.gov/18639629/)
67. Nizri E, Brenner T. Modulation of inflammatory pathways by the immune cholinergic system. *Amino Acids.* 2013; 45:73–85.
<https://doi.org/10.1007/s00726-011-1192-8>
PMID:[22194043](https://pubmed.ncbi.nlm.nih.gov/22194043/)
68. Gamage R, Wagnon I, Rossetti I, Childs R, Niedermayer G, Chesworth R, Gyengesi E. Cholinergic Modulation of Glial Function During Aging and Chronic Neuroinflammation. *Front Cell Neurosci.* 2020; 14:577912.
<https://doi.org/10.3389/fncel.2020.577912>
PMID:[33192323](https://pubmed.ncbi.nlm.nih.gov/33192323/)
69. Borovikova LV, Ivanova S, Zhang M, Yang H, Botchkina GI, Watkins LR, Wang H, Abumrad N, Eaton JW, Tracey KJ. Vagus nerve stimulation attenuates the systemic inflammatory response to endotoxin. *Nature.* 2000; 405:458–62.
<https://doi.org/10.1038/35013070> PMID:[10839541](https://pubmed.ncbi.nlm.nih.gov/10839541/)
70. Liu EY, Xia Y, Kong X, Guo MS, Yu AX, Zheng BZ, Mak S, Xu ML, Tsim KW. Interacting with $\alpha 7$ nAChR is a new mechanism for AChE to enhance the inflammatory response in macrophages. *Acta Pharm Sin B.* 2020; 10:1926–42.
<https://doi.org/10.1016/j.apsb.2020.05.005>
PMID:[33163344](https://pubmed.ncbi.nlm.nih.gov/33163344/)
71. Moreira NC, Lima JE, Marchiori MF, Carvalho I, Sakamoto-Hojo ET. Neuroprotective Effects of Cholinesterase Inhibitors: Current Scenario in Therapies for Alzheimer's Disease and Future Perspectives. *J Alzheimers Dis Rep.* 2022; 6:177–93.
<https://doi.org/10.3233/ADR-210061>
PMID:[35591949](https://pubmed.ncbi.nlm.nih.gov/35591949/)
72. Benfante R, Di Lascio S, Cardani S, Fornasari D. Acetylcholinesterase inhibitors targeting the cholinergic anti-inflammatory pathway: a new therapeutic perspective in aging-related disorders. *Aging Clin Exp Res.* 2021; 33:823–34.
<https://doi.org/10.1007/s40520-019-01359-4>
PMID:[31583530](https://pubmed.ncbi.nlm.nih.gov/31583530/)
73. Raffaele M, Vinciguerra M. The costs and benefits of senotherapeutics for human health. *Lancet Healthy Longev.* 2022; 3:e67–77.
[https://doi.org/10.1016/S2666-7568\(21\)00300-7](https://doi.org/10.1016/S2666-7568(21)00300-7)
PMID:[36098323](https://pubmed.ncbi.nlm.nih.gov/36098323/)
74. Riessland M, Orr ME. Translating the Biology of Aging into New Therapeutics for Alzheimer's Disease: Senolytics. *J Prev Alzheimers Dis.* 2023; 10:633–46.
<https://doi.org/10.14283/jpad.2023.104>
PMID:[37874084](https://pubmed.ncbi.nlm.nih.gov/37874084/)
75. Zs-Nagy I. Pharmacological interventions against aging through the cell plasma membrane: a review of the experimental results obtained in animals and humans. *Ann N Y Acad Sci.* 2002.
<https://doi.org/10.1111/j.1749-6632.2002.tb02102.x>
PMID:[11976205](https://pubmed.ncbi.nlm.nih.gov/11976205/)
76. Bussian TJ, Aziz A, Meyer CF, Swenson BL, van Deursen JM, Baker DJ. Clearance of senescent glial cells prevents tau-dependent pathology and cognitive decline. *Nature.* 2018; 562:578–82.
<https://doi.org/10.1038/s41586-018-0543-y>
PMID:[30232451](https://pubmed.ncbi.nlm.nih.gov/30232451/)
77. Musi N, Valentine JM, Sickora KR, Baeuerle E, Thompson CS, Shen Q, Orr ME. Tau protein aggregation is associated with cellular senescence in the brain. *Aging Cell.* 2018; 17:e12840.
<https://doi.org/10.1111/accel.12840> PMID:[30126037](https://pubmed.ncbi.nlm.nih.gov/30126037/)
78. Zhang P, Kishimoto Y, Grammatikakis I, Gottimukkala K, Cutler RG, Zhang S, Abdelmohsen K, Bohr VA, Misra Sen J, Gorospe M, Mattson MP. Senolytic therapy alleviates A β -associated oligodendrocyte progenitor cell senescence and cognitive deficits in an Alzheimer's disease model. *Nat Neurosci.* 2019; 22:719–28.
<https://doi.org/10.1038/s41593-019-0372-9>
PMID:[30936558](https://pubmed.ncbi.nlm.nih.gov/30936558/)
79. Hu Y, Fryatt GL, Ghorbani M, Obst J, Menassa DA, Martin-Estebane M, Muntslag TA, Olmos-Alonso A, Guerrero-Carrasco M, Thomas D, Cragg MS, Gomez-Nicola D. Replicative senescence dictates the emergence of disease-associated microglia and contributes to A β pathology. *Cell Rep.* 2021; 35:109228.
<https://doi.org/10.1016/j.celrep.2021.109228>
PMID:[34107254](https://pubmed.ncbi.nlm.nih.gov/34107254/)
80. Zhu Y, Tchkonina T, Fuhrmann-Stroissnigg H, Dai HM, Ling YY, Stout MB, Pirtskhalava T, Giorgadze N, Johnson KO, Giles CB, Wren JD, Niedernhofer LJ, Robbins PD,

- Kirkland JL. Identification of a novel senolytic agent, navitoclax, targeting the Bcl-2 family of anti-apoptotic factors. *Aging Cell*. 2016; 15:428–35.
<https://doi.org/10.1111/accel.12445>
PMID:[26711051](https://pubmed.ncbi.nlm.nih.gov/26711051/)
81. Chaib S, Tchkonja T, Kirkland JL. Cellular senescence and senolytics: the path to the clinic. *Nat Med*. 2022; 28:1556–68.
<https://doi.org/10.1038/s41591-022-01923-y>
PMID:[35953721](https://pubmed.ncbi.nlm.nih.gov/35953721/)
82. Nandy K, Bourne GH. Effect of centrophenoxine on the lipofuscin pigments in the neurones of senile guinea-pigs. *Nature*. 1966; 210:313–4.
<https://doi.org/10.1038/210313a0> PMID:[4380940](https://pubmed.ncbi.nlm.nih.gov/4380940/)
83. Nandy K. Centrophenoxine: effects on aging mammalian brain. *J Am Geriatr Soc*. 1978; 26:74–81.
<https://doi.org/10.1111/j.1532-5415.1978.tb02544.x>
PMID:[342588](https://pubmed.ncbi.nlm.nih.gov/342588/)
84. Bhalla P, Nehru B. Modulatory effects of centrophenoxine on different regions of ageing rat brain. *Exp Gerontol*. 2005; 40:801–6.
<https://doi.org/10.1016/j.exger.2005.06.016>
PMID:[16137852](https://pubmed.ncbi.nlm.nih.gov/16137852/)
85. Pohanka M. Inhibitors of acetylcholinesterase and butyrylcholinesterase meet immunity. *Int J Mol Sci*. 2014; 15:9809–25.
<https://doi.org/10.3390/ijms15069809>
PMID:[24893223](https://pubmed.ncbi.nlm.nih.gov/24893223/)
86. Sands D, Davis A, Banfield S, Pottie IR, Darvesh S. Solvents and detergents compatible with enzyme kinetic studies of cholinesterases. *Chem Biol Interact*. 2023; 383:110667.
<https://doi.org/10.1016/j.cbi.2023.110667>
PMID:[37579937](https://pubmed.ncbi.nlm.nih.gov/37579937/)
87. Orhan I, Kartal M, Tosun F, Sener B. Screening of various phenolic acids and flavonoid derivatives for their anticholinesterase potential. *Z Naturforsch C J Biosci*. 2007; 62:829–32.
<https://doi.org/10.1515/znc-2007-11-1210>
PMID:[18274286](https://pubmed.ncbi.nlm.nih.gov/18274286/)
88. Darvesh S, Banfield S, Dufour M, Forrestall KL, Maillet H, Reid GA, Sands D, Pottie IR. A method for the efficient evaluation of substrate-based cholinesterase imaging probes for Alzheimer's disease. *J Enzyme Inhib Med Chem*. 2023; 38:2225797.
<https://doi.org/10.1080/14756366.2023.2225797>
PMID:[38061987](https://pubmed.ncbi.nlm.nih.gov/38061987/)
89. Rodríguez-Arce E, Saldías M. Antioxidant properties of flavonoid metal complexes and their potential inclusion in the development of novel strategies for the treatment against neurodegenerative diseases. *Biomed Pharmacother*. 2021; 143:112236.
<https://doi.org/10.1016/j.biopha.2021.112236>
PMID:[34649360](https://pubmed.ncbi.nlm.nih.gov/34649360/)
90. Maher P. Modulation of the Neuroprotective and Anti-inflammatory Activities of the Flavonol Fisetin by the Transition Metals Iron and Copper. *Antioxidants (Basel)*. 2020; 9:1113.
<https://doi.org/10.3390/antiox9111113>
PMID:[33187316](https://pubmed.ncbi.nlm.nih.gov/33187316/)
91. Cheung J, Gary EN, Shiomi K, Rosenberry TL. Structures of human acetylcholinesterase bound to dihydro-tanshinone I and territrein B show peripheral site flexibility. *ACS Med Chem Lett*. 2013; 4:1091–6.
<https://doi.org/10.1021/ml400304w>
PMID:[24900610](https://pubmed.ncbi.nlm.nih.gov/24900610/)
92. Brus B, Košak U, Turk S, Pišlar A, Coquelle N, Kos J, Stojan J, Colletier JP, Gobec S. Discovery, biological evaluation, and crystal structure of a novel nanomolar selective butyrylcholinesterase inhibitor. *J Med Chem*. 2014; 57:8167–79.
<https://doi.org/10.1021/jm501195e>
PMID:[25226236](https://pubmed.ncbi.nlm.nih.gov/25226236/)
93. Saxena A, Redman AM, Jiang X, Lockridge O, Doctor BP. Differences in active-site gorge dimensions of cholinesterases revealed by binding of inhibitors to human butyrylcholinesterase. *Chem Biol Interact*. 1999; 119–120:61–9.
[https://doi.org/10.1016/s0009-2797\(99\)00014-9](https://doi.org/10.1016/s0009-2797(99)00014-9)
PMID:[10421439](https://pubmed.ncbi.nlm.nih.gov/10421439/)
94. Kongkaew N, Hengphasatporn K, Shigeta Y, Rungrotmongkol T, Harada R. Preferential Door for Ligand Binding and Unbinding Pathways in Inhibited Human Acetylcholinesterase. *J Phys Chem Lett*. 2024; 15:5696–704.
<https://doi.org/10.1021/acs.jpcclett.4c00514>
PMID:[38768263](https://pubmed.ncbi.nlm.nih.gov/38768263/)
95. Xu Y, Colletier JP, Weik M, Qin G, Jiang H, Silman I, Sussman JL. Long route or shortcut? A molecular dynamics study of traffic of thiocholine within the active-site gorge of acetylcholinesterase. *Biophys J*. 2010; 99:4003–11.
<https://doi.org/10.1016/j.bpj.2010.10.047>
PMID:[21156143](https://pubmed.ncbi.nlm.nih.gov/21156143/)
96. Wiesner J, Kříž Z, Kuča K, Jun D, Koča J. Influence of the acetylcholinesterase active site protonation on omega loop and active site dynamics. *J Biomol Struct Dyn*. 2010; 28:393–403.
<https://doi.org/10.1080/07391102.2010.10507368>
PMID:[20919754](https://pubmed.ncbi.nlm.nih.gov/20919754/)
97. Gilson MK, Straatsma TP, McCammon JA, Ripoll DR, Faerman CH, Axelsen PH, Silman I, Sussman JL. Open “back door” in a molecular dynamics simulation of acetylcholinesterase. *Science*. 1994; 263:1276–8.

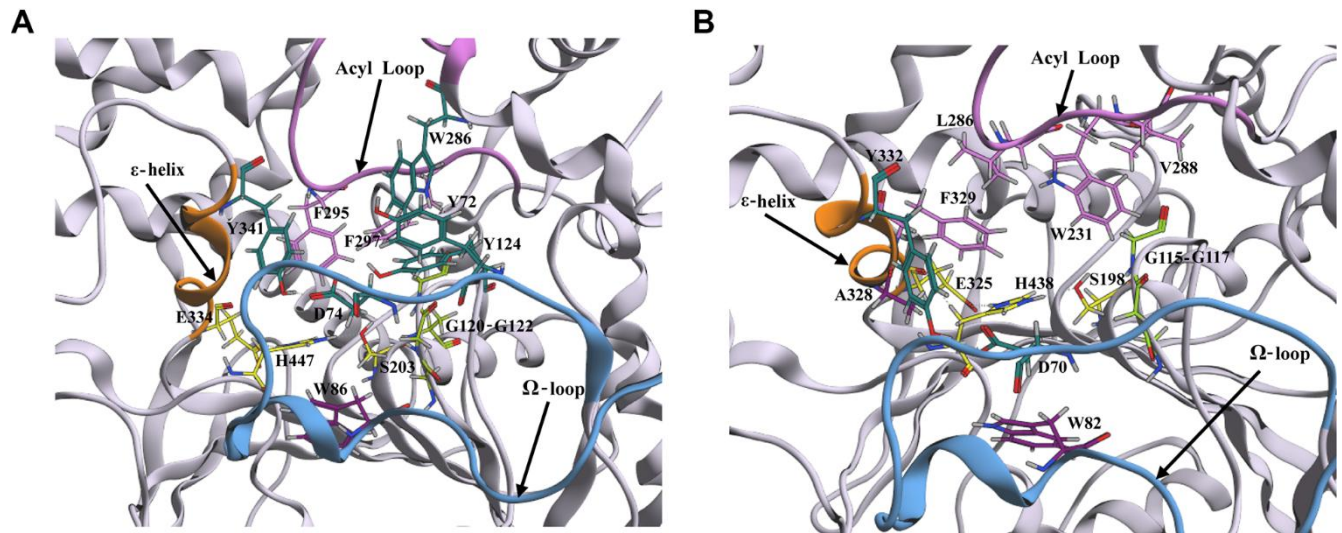
- <https://doi.org/10.1126/science.8122110>
PMID:8122110
98. Chinnadurai RK, Saravanaraman P, Boopathy R. Understanding the molecular mechanism of aryl acylamidase activity of acetylcholinesterase - An *in silico* study. Arch Biochem Biophys. 2015; 580:1–13.
<https://doi.org/10.1016/j.abb.2015.06.002>
PMID:26072115
99. Hetényi C, van der Spoel D. Blind docking of drug-sized compounds to proteins with up to a thousand residues. FEBS Lett. 2006; 580:1447–50.
<https://doi.org/10.1016/j.febslet.2006.01.074>
PMID:16460734
100. Bender BJ, Gahbauer S, Lutgens A, Lyu J, Webb CM, Stein RM, Fink EA, Balius TE, Carlsson J, Irwin JJ, Shoichet BK. A practical guide to large-scale docking. Nat Protoc. 2021; 16:4799–832.
<https://doi.org/10.1038/s41596-021-00597-z>
PMID:34561691
101. Maden SF, Sezer S, Acuner SE. Fundamentals of Molecular Docking and Comparative Analysis of Protein–Small-Molecule Docking Approaches. In: Istifli ES, ed. Molecular Docking - Recent Advances. (Rijeka, Croatia: IntechOpen). 2023; 1–24.
102. Hetényi C, van der Spoel D. Efficient docking of peptides to proteins without prior knowledge of the binding site. Protein Sci. 2002; 11:1729–37.
<https://doi.org/10.1110/ps.0202302>
PMID:12070326
103. Hetényi C, van der Spoel D. Toward prediction of functional protein pockets using blind docking and pocket search algorithms. Protein Sci. 2011; 20:880–93.
<https://doi.org/10.1002/pro.618> PMID:21413095
104. Bálint M, Jeszenői N, Horváth I, van der Spoel D, Hetényi C. Systematic exploration of multiple drug binding sites. J Cheminform. 2017; 9:65.
<https://doi.org/10.1186/s13321-017-0255-6>
PMID:29282592
105. Waldrop GL. A qualitative approach to enzyme inhibition. Biochem Mol Biol Educ. 2009; 37:11–5.
<https://doi.org/10.1002/bmb.20243>
PMID:21567682
106. Faria OW, de Aguiar MS, de Mello JE, Alvez FL, Luduvico KP, Garcia DN, Schneider A, Masternak MM, Spanevello RM, Stefanello FM. Senolytics prevent age-associated changes in female mice brain. Neurosci Lett. 2024; 826:137730.
<https://doi.org/10.1016/j.neulet.2024.137730>
PMID:38485080
107. Inestrosa NC, Alvarez A, Pérez CA, Moreno RD, Vicente M, Linker C, Casanueva OI, Soto C, Garrido J. Acetylcholinesterase accelerates assembly of amyloid-beta-peptides into Alzheimer's fibrils: possible role of the peripheral site of the enzyme. Neuron. 1996; 16:881–91.
[https://doi.org/10.1016/s0896-6273\(00\)80108-7](https://doi.org/10.1016/s0896-6273(00)80108-7)
PMID:8608006
108. Johnson G, Moore SW. The adhesion function on acetylcholinesterase is located at the peripheral anionic site. Biochem Biophys Res Commun. 1999; 258:758–62.
<https://doi.org/10.1006/bbrc.1999.0705>
PMID:10329459
109. Bartolini M, Bertucci C, Cavrini V, Andrisano V. beta-Amyloid aggregation induced by human acetylcholinesterase: inhibition studies. Biochem Pharmacol. 2003; 65:407–16.
[https://doi.org/10.1016/s0006-2952\(02\)01514-9](https://doi.org/10.1016/s0006-2952(02)01514-9)
PMID:12527333
110. Kumar R, Nordberg A, Darreh-Shori T. Amyloid- β peptides act as allosteric modulators of cholinergic signalling through formation of soluble BA β ACs. Brain. 2016; 139:174–92.
<https://doi.org/10.1093/brain/awv318>
PMID:26525916
111. Zueva IV, Vasilieva EA, Gaynanova GA, Moiseenko AV, Burtseva AD, Boyko KM, Zakharova LY, Petrov KA. Can Activation of Acetylcholinesterase by β -Amyloid Peptide Decrease the Effectiveness of Cholinesterase Inhibitors? Int J Mol Sci. 2023; 24:16395.
<https://doi.org/10.3390/ijms242216395>
PMID:38003588
112. Mukhametgalieva AR, Nemtarev AV, Sykaev VV, Pashirova TN, Masson P. Activation/Inhibition of Cholinesterases by Excess Substrate: Interpretation of the Phenomenological b Factor in Steady-State Rate Equation. Int J Mol Sci. 2023; 24:10472.
<https://doi.org/10.3390/ijms241310472>
PMID:37445649
113. Fang L, Pan Y, Muzyka JL, Zhan CG. Active site gating and substrate specificity of butyrylcholinesterase and acetylcholinesterase: insights from molecular dynamics simulations. J Phys Chem B. 2011; 115:8797–805.
<https://doi.org/10.1021/jp112030p>
PMID:21682268
114. Roca C, Requena C, Sebastián-Pérez V, Malhotra S, Radoux C, Pérez C, Martínez A, Antonio Páez J, Blundell TL, Campillo NE. Identification of new allosteric sites and modulators of AChE through computational and experimental tools. J Enzyme Inhib Med Chem. 2018; 33:1034–47.
<https://doi.org/10.1080/14756366.2018.1476502>
PMID:29873262

115. Carlacci L, Millard CB, Olson MA. Conformational energy landscape of the acyl pocket loop in acetylcholinesterase: a Monte Carlo-generalized Born model study. *Biophys Chem.* 2004; 111:143–57. <https://doi.org/10.1016/j.bpc.2004.05.007> PMID:[15381312](https://pubmed.ncbi.nlm.nih.gov/15381312/)
116. Hörnberg A, Tunemalm AK, Ekström F. Crystal structures of acetylcholinesterase in complex with organophosphorus compounds suggest that the acyl pocket modulates the aging reaction by precluding the formation of the trigonal bipyramidal transition state. *Biochemistry.* 2007; 46:4815–25. <https://doi.org/10.1021/bi0621361> PMID:[17402711](https://pubmed.ncbi.nlm.nih.gov/17402711/)
117. Bourne Y, Taylor P, Radić Z, Marchot P. Structural insights into ligand interactions at the acetylcholinesterase peripheral anionic site. *EMBO J.* 2003; 22:1–12. <https://doi.org/10.1093/emboj/cdg005> PMID:[12505979](https://pubmed.ncbi.nlm.nih.gov/12505979/)
118. Saxena A, Fedorko JM, Vinayaka CR, Medhekar R, Radić Z, Taylor P, Lockridge O, Doctor BP. Aromatic amino-acid residues at the active and peripheral anionic sites control the binding of E2020 (Aricept) to cholinesterases. *Eur J Biochem.* 2003; 270:4447–58. <https://doi.org/10.1046/j.1432-1033.2003.03837.x> PMID:[14622273](https://pubmed.ncbi.nlm.nih.gov/14622273/)
119. Branduardi D, Gervasio FL, Cavalli A, Recanatini M, Parrinello M. The role of the peripheral anionic site and cation- π interactions in the ligand penetration of the human AChE gorge. *J Am Chem Soc.* 2005; 127:9147–55. <https://doi.org/10.1021/ja0512780> PMID:[15969593](https://pubmed.ncbi.nlm.nih.gov/15969593/)
120. 2024 Alzheimer's disease facts and figures. *Alzheimers Dement.* 2024; 20:3708–821. <https://doi.org/10.1002/alz.13809> PMID:[38689398](https://pubmed.ncbi.nlm.nih.gov/38689398/)
121. Barnes LL, Wilson RS, Bienias JL, Schneider JA, Evans DA, Bennett DA. Sex differences in the clinical manifestations of Alzheimer disease pathology. *Arch Gen Psychiatry.* 2005; 62:685–91. <https://doi.org/10.1001/archpsyc.62.6.685> PMID:[15939846](https://pubmed.ncbi.nlm.nih.gov/15939846/)
122. Sinforiani E, Citterio A, Zucchella C, Bono G, Corbetta S, Merlo P, Mauri M. Impact of gender differences on the outcome of Alzheimer's disease. *Dement Geriatr Cogn Disord.* 2010; 30:147–54. <https://doi.org/10.1159/000318842> PMID:[20733307](https://pubmed.ncbi.nlm.nih.gov/20733307/)
123. Reid GA, Darvesh S. Butyrylcholinesterase-knockout reduces brain deposition of fibrillar β -amyloid in an Alzheimer mouse model. *Neuroscience.* 2015; 298:424–35. <https://doi.org/10.1016/j.neuroscience.2015.04.039> PMID:[25931333](https://pubmed.ncbi.nlm.nih.gov/25931333/)
124. Darvesh S, Reid GA. Reduced fibrillar β -amyloid in subcortical structures in a butyrylcholinesterase-knockout Alzheimer disease mouse model. *Chem Biol Interact.* 2016; 259:307–12. <https://doi.org/10.1016/j.cbi.2016.04.022> PMID:[27091549](https://pubmed.ncbi.nlm.nih.gov/27091549/)
125. Morley JE, Farr SA, Kumar VB, Armbrecht HJ. The SAMP8 mouse: a model to develop therapeutic interventions for Alzheimer's disease. *Curr Pharm Des.* 2012; 18:1123–30. <https://doi.org/10.2174/138161212799315795> PMID:[22288401](https://pubmed.ncbi.nlm.nih.gov/22288401/)
126. Morley JE, Kumar VB, Bernardo AE, Farr SA, Uezu K, Tumosa N, Flood JF. Beta-amyloid precursor polypeptide in SAMP8 mice affects learning and memory. *Peptides.* 2000; 21:1761–7. [https://doi.org/10.1016/s0196-9781\(00\)00342-9](https://doi.org/10.1016/s0196-9781(00)00342-9) PMID:[11150635](https://pubmed.ncbi.nlm.nih.gov/11150635/)
127. Darvesh S, Cash MK, Reid GA, Martin E, Mitnitski A, Geula C. Butyrylcholinesterase is associated with β -amyloid plaques in the transgenic APPSWE/PSEN1dE9 mouse model of Alzheimer disease. *J Neuropathol Exp Neurol.* 2012; 71:2–14. <https://doi.org/10.1097/NEN.0b013e31823cc7a6> PMID:[22157615](https://pubmed.ncbi.nlm.nih.gov/22157615/)
128. Koelle GB. The histochemical localization of cholinesterases in the central nervous system of the rat. *J Comp Neurol.* 1954; 100:211–35. <https://doi.org/10.1002/cne.901000108> PMID:[13130712](https://pubmed.ncbi.nlm.nih.gov/13130712/)
129. Roessmann U, Friede RL. Changes in butyryl cholinesterase activity in reactive glia. *Neurology.* 1966; 16:123–9. https://doi.org/10.1212/wnl.16.2_part_1.123 PMID:[5948501](https://pubmed.ncbi.nlm.nih.gov/5948501/)
130. Darvesh S, Leblanc AM, Macdonald IR, Reid GA, Bhan V, Macaulay RJ, Fisk JD. Butyrylcholinesterase activity in multiple sclerosis neuropathology. *Chem Biol Interact.* 2010; 187:425–31. <https://doi.org/10.1016/j.cbi.2010.01.037> PMID:[20122907](https://pubmed.ncbi.nlm.nih.gov/20122907/)
131. Di Pinto G, Di Bari M, Martin-Alvarez R, Sperduti S, Serrano-Acedo S, Gatta V, Tata AM, Mengod G. Comparative study of the expression of cholinergic system components in the CNS of experimental autoimmune encephalomyelitis mice: Acute vs. remitting phase. *Eur J Neurosci.* 2018; 48:2165–81. <https://doi.org/10.1111/ejn.14125> PMID:[30144326](https://pubmed.ncbi.nlm.nih.gov/30144326/)
132. Thorne MW, Cash MK, Reid GA, Burley DE, Luke D, Pottie IR, Darvesh S. Imaging Butyrylcholinesterase in

- Multiple Sclerosis. *Mol Imaging Biol.* 2021; 23:127–38.
<https://doi.org/10.1007/s11307-020-01540-6>
PMID:[32926288](https://pubmed.ncbi.nlm.nih.gov/32926288/)
133. Fernández A, Quintana E, Velasco P, Moreno-Jimenez B, de Andrés B, Gaspar ML, Liste I, Vilar M, Mira H, Cano E. Senescent accelerated prone 8 (SAMP8) mice as a model of age dependent neuroinflammation. *J Neuroinflammation.* 2021; 18:75.
<https://doi.org/10.1186/s12974-021-02104-3>
PMID:[33736657](https://pubmed.ncbi.nlm.nih.gov/33736657/)
134. Tha KK, Okuma Y, Miyazaki H, Murayama T, Uehara T, Hatakeyama R, Hayashi Y, Nomura Y. Changes in expressions of proinflammatory cytokines IL-1beta, TNF-alpha and IL-6 in the brain of senescence accelerated mouse (SAM) P8. *Brain Res.* 2000; 885:25–31.
[https://doi.org/10.1016/s0006-8993\(00\)02883-3](https://doi.org/10.1016/s0006-8993(00)02883-3)
PMID:[11121526](https://pubmed.ncbi.nlm.nih.gov/11121526/)
135. Greig NH, Utsuki T, Ingram DK, Wang Y, Pepeu G, Scali C, Yu QS, Mamczarz J, Holloway HW, Giordano T, Chen D, Furukawa K, Sambamurti K, et al. Selective butyrylcholinesterase inhibition elevates brain acetylcholine, augments learning and lowers Alzheimer beta-amyloid peptide in rodent. *Proc Natl Acad Sci USA.* 2005; 102:17213–18.
<https://doi.org/10.1073/pnas.0508575102>
PMID:[16275899](https://pubmed.ncbi.nlm.nih.gov/16275899/)
136. Lunin SM, Novoselova EG, Glushkova OV, Parfenyuk SB, Novoselova TV, Khrenov MO. Cell Senescence and Central Regulators of Immune Response. *Int J Mol Sci.* 2022; 23:4109.
<https://doi.org/10.3390/ijms23084109>
PMID:[35456927](https://pubmed.ncbi.nlm.nih.gov/35456927/)
137. Ellman GL, Courtney KD, ANDRES V Jr, Feather-Stone RM. A new and rapid colorimetric determination of acetylcholinesterase activity. *Biochem Pharmacol.* 1961; 7:88–95.
[https://doi.org/10.1016/0006-2952\(61\)90145-9](https://doi.org/10.1016/0006-2952(61)90145-9)
PMID:[13726518](https://pubmed.ncbi.nlm.nih.gov/13726518/)
138. Darvesh S, Hopkins DA. Differential distribution of butyrylcholinesterase and acetylcholinesterase in the human thalamus. *J Comp Neurol.* 2003; 463:25–43.
<https://doi.org/10.1002/cne.10751> PMID:[12811800](https://pubmed.ncbi.nlm.nih.gov/12811800/)
139. McKhann GM, Knopman DS, Chertkow H, Hyman BT, Jack CR Jr, Kawas CH, Klunk WE, Koroshetz WJ, Manly JJ, Mayeux R, Mohs RC, Morris JC, Rossor MN, et al. The diagnosis of dementia due to Alzheimer’s disease: recommendations from the National Institute on Aging-Alzheimer’s Association workgroups on diagnostic guidelines for Alzheimer’s disease. *Alzheimers Dement.* 2011; 7:263–9.
<https://doi.org/10.1016/j.jalz.2011.03.005>
PMID:[21514250](https://pubmed.ncbi.nlm.nih.gov/21514250/)
140. Hyman BT, Phelps CH, Beach TG, Bigio EH, Cairns NJ, Carrillo MC, Dickson DW, Duyckaerts C, Frosch MP, Masliah E, Mirra SS, Nelson PT, Schneider JA, et al. National Institute on Aging-Alzheimer’s Association guidelines for the neuropathologic assessment of Alzheimer’s disease. *Alzheimers Dement.* 2012; 8:1–13.
<https://doi.org/10.1016/j.jalz.2011.10.007>
PMID:[22265587](https://pubmed.ncbi.nlm.nih.gov/22265587/)
141. Braak H, Alafuzoff I, Arzberger T, Kretschmar H, Del Tredici K. Staging of Alzheimer disease-associated neurofibrillary pathology using paraffin sections and immunocytochemistry. *Acta Neuropathol.* 2006; 112:389–404.
<https://doi.org/10.1007/s00401-006-0127-z>
PMID:[16906426](https://pubmed.ncbi.nlm.nih.gov/16906426/)
142. Mirra SS, Heyman A, McKeel D, Sumi SM, Crain BJ, Brownlee LM, Vogel FS, Hughes JP, van Belle G, Berg L. The Consortium to Establish a Registry for Alzheimer’s Disease (CERAD). Part II. Standardization of the neuropathologic assessment of Alzheimer’s disease. *Neurology.* 1991; 41:479–86.
<https://doi.org/10.1212/wnl.41.4.479>
PMID:[2011243](https://pubmed.ncbi.nlm.nih.gov/2011243/)
143. Karnovsky MJ, Roots L. A “DIRECT-COLORING” THIOCHOLINE METHOD FOR CHOLINESTERASES. *J Histochem Cytochem.* 1964; 12:219–21.
<https://doi.org/10.1177/12.3.219>
PMID:[14187330](https://pubmed.ncbi.nlm.nih.gov/14187330/)
144. Forrestall KL, Burley DE, Cash MK, Pottie IR, Darvesh S. Phenothiazines as dual inhibitors of SARS-CoV-2 main protease and COVID-19 inflammation. *Can J Chem.* 2021; 99:801–11.
<https://doi.org/10.1139/cjc-2021-0139>
145. Forrestall K, Pringle ES, Sands D, Duguay BA, Farewell B, Woldemariam T, Falzarano D, Pottie I, McCormick C, Darvesh S. A phenothiazine urea derivative broadly inhibits coronavirus replication via viral protease inhibition. *Antiviral Res.* 2023; 220:105758.
<https://doi.org/10.1016/j.antiviral.2023.105758>
PMID:[38008194](https://pubmed.ncbi.nlm.nih.gov/38008194/)
146. Berman HM, Westbrook J, Feng Z, Gilliland G, Bhat TN, Weissig H, Shindyalov IN, Bourne PE. The Protein Data Bank. *Nucleic Acids Res.* 2000; 28:235–42.
<https://doi.org/10.1093/nar/28.1.235>
PMID:[10592235](https://pubmed.ncbi.nlm.nih.gov/10592235/)
147. Forrestall KL, Burley DE, Cash MK, Pottie IR, Darvesh S. 2-Pyridone natural products as inhibitors of SARS-CoV-2 main protease. *Chem Biol Interact.* 2021; 335:109348.
<https://doi.org/10.1016/j.cbi.2020.109348>
PMID:[33278462](https://pubmed.ncbi.nlm.nih.gov/33278462/)

SUPPLEMENTARY MATERIALS

Supplementary Figure



Supplementary Figure 1. Features and key amino acid residues of the active site gorge of acetylcholinesterase (AChE, **(A)** PDB: 4M0E, 2.00 Å [90] and butyrylcholinesterase (BChE, **(B)** PDB: 4TPK, 2.70 Å). The catalytic triad is shown in yellow ((**A**) S203, E334, H447; (**B**) S198, E325, H438), acyl binding pocket residues are shown in pink ((**A**) F295, F297; (**B**) W231, L286, V288, F329), peripheral anionic site residues are shown in teal ((**A**) Y72, D76, Y124, W286, Y341; (**B**) D70, Y332), π -cationic site residues are shown in purple ((**A**) W86; (**B**) W82, A328), and oxyanion hole residues are shown in lime green ((**A**) G120-G122; (**B**) G115-G117). Acyl loop, Ω -loop, and ϵ -helix are shown as pink, blue, and orange ribbon structures, respectively. Images were generated with Molecular Operating Environment 2022.02 (Chemical Computing Group ULC, Montreal, Quebec, Canada).

Supplementary Tables

Supplementary Table 1. Enzyme binding sites identified in blind docking experiments with acetylcholinesterase (AChE; PDB: 4M0E) [90] and butyrylcholinesterase (BChE; PDB: 4TPK) [91] for senolytic and nootropic drugs 1-6 using Molecular Operating Environment 2022.02 (Chemical Computing Group ULC, Montreal, Quebec, Canada).

Compound	AChE blind docks					BChE blind docks				
	Site I	Site II	Site III	Site IV	Site V	Site I	Site II	Site III	Site IV	Site V
1	^a	12/15	3/15	–	–	–	6/15	9/15	–	–
2	–	6/15	6/15	–	3/15	–	–	12/15	–	3/15
3	12/15	3/15	–	–	–	3/15	–	9/15	3/15	–
4	6/15	9/15	–	–	–	9/15	–	6/15	–	–
5	3/15	9/15	3/15	–	–	–	–	15/15	–	–
6	6/15	3/15	–	6/15	–	6/15	–	6/15	–	3/15

^aThe number of docking poses for 1-6 at each indicated binding site (enzyme active site gorge (I), cholinesterase (ChE) pocket behind acyl loop (II), pocket behind ChE catalytic glutamate (III), pocket behind key ChE active site tryptophan (Back Door, IV), or other site (V)) are shown from triplicate blind docking experiments (3 x 5 poses).

Supplementary Table 2. *In silico* predicted inhibition constants (K_i values) for compounds 1-6 with acetylcholinesterase (AChE; PDB: 4M0E, 2.00 Å) [91] and butyrylcholinesterase (BChE; PDB: 4PTK, 2.70 Å) [92].

Compound	Predicted AChE K_i^a (μM)	Predicted BChE K_i^a (μM)
1	27.63*	0.35*
	126.20†	3.04†
	16.17*	1.04†
2	61.33†	5.09‡
	110.20‡	
	5.32	16.49
3	243.12*	32.46†
		55.33◇
		16.66
4	5.14	24.76†
	177.24*	
	0.73	10.30†
5	89.63*	
	361.53†	
	11.92	16.14
6	191.53*	42.96†
	299.72◇	48.38‡

^aSites selected for directed docking were the enzyme active site (Site I, no symbol) or alternate sites (II-V) identified from blind docking experiments (II, *; III, †; IV, ◇; V, ‡).

Molecular docking experiments were completed using Molecular Operating Environment 2022.02 (Chemical Computing Group ULC, Montreal, Quebec, Canada).

Supplementary Table 3. *In silico* binding interactions of senolytics 1-5 and nootropic 6 with acetylcholinesterase (AChE, PDB: 4MOE) [91] and butyrylcholinesterase (BChE, PDB: 4TPK) [92] for top site-directed docking poses at cholinesterase (ChE) binding sites I-V.

Compound	Enzyme	Binding site (I-V)	Bonding residues ^a	Bond type ^a	Bond length ^a (Å)	Enzyme structure location ^b	
1	AChE	II	N233	H-acceptor	3.08	Bottom wall of site gorge	
			R296	H-acceptor	2.89	Acyl Loop	
			R296	H-acceptor	3.21	Acyl Loop	
		III	K332	H-acceptor	3.00	Site gorge wall	
			R525	H-acceptor	3.19	Site gorge wall	
			R525	π -H	4.03	Site gorge wall	
	BChE	II	S235	H-acceptor	3.03	Acyl Loop	
			S235	H-acceptor	3.04	Acyl Loop	
			R242	H-acceptor	3.48	Acyl Loop	
		III	V288	π -H	3.95	Acyl Loop, ABP	
			F357	H-donor	3.16	Site gorge wall	
			N397	H-acceptor	3.31	Site gorge wall	
		AChE	III	D324	H-donor	2.92	Site gorge wall, beside ϵ -helix
				R296	H-acceptor	3.06	Acyl Loop
				R296	H-acceptor	3.21	Acyl Loop
2	AChE	III	R521	H-acceptor	3.06	Site gorge wall	
			R525	H-acceptor	3.50	Site gorge wall	
			Q181	π -H	3.92	Site gorge wall	
		BChE	III	K323	H-acceptor	3.05	Site gorge wall
				V377	π -H	4.69	Site gorge wall
				D391	H-donor	2.99	Site gorge wall
	AChE	V	-	-	-	-	
			I	Y72	H-donor	2.88	Ω -loop, PAS
				W86	H-donor	3.09	Ω -loop, PCS
		W86		π - π	3.77	Ω -loop, PCS	
		BChE	II	W86	π - π	3.79	Ω -loop, PCS
				E202	H-donor	2.76	Bottom wall of site gorge
				R247	H-acceptor	3.02	Site gorge wall
		AChE	I	W82	π - π	3.74	Ω -loop, PCS
				W82	π - π	3.80	Ω -loop, PCS
W82	H-donor			2.92	Ω -loop, PCS		
BChE	III		E197	H-donor	2.78	Bottom wall of site gorge	
			Y373	π -H	3.99	Site gorge wall	
			E387	H-donor	2.74	Site gorge wall	
AChE	IV		D391	H-donor	2.89	Site gorge wall	
			R515	H-acceptor	3.47	Site gorge wall	
			H77	π -H	3.49	Ω -loop	
	BChE	I	M81	H-donor	3.81	Ω -loop	
			W86	π - π	3.79	Ω -loop, PCS	
			W86	π - π	3.86	Ω -loop, PCS	
	AChE	II	E202	H-donor	2.78	Bottom wall of site gorge	
			R296	π -cation	3.48	Acyl Loop	
			R296	π -cation	3.94	Acyl Loop	
BChE		I	W82	π - π	3.79	Ω -loop, PCS	
			W82	π - π	3.81	Ω -loop, PCS	

5	AChE	III	E197	H-donor	2.77	Bottom wall of site gorge	
			Y373	π -H	3.99	Site gorge wall	
			E387	H-donor	2.74	Site gorge wall	
			D391	H-donor	2.89	Site gorge wall	
			R515	H-acceptor	3.47	Site gorge wall	
			I	Y341	H- π	4.23	ϵ -helix, PAS
				II	N233	H-donor	3.66
		III	S399		H-acceptor	2.96	Site gorge wall
			D400	H-donor	2.82	Site gorge wall	
			W442	H-donor	2.86	Opposite S336 of ϵ -helix	
		BChE	III	R525	π -cation	3.75	Site gorge wall
				-	-	-	-
			I	Y341	H- π	3.82	ϵ -helix, PAS
				H447	π -H	3.98	Catalytic Triad
AChE	II		R247	H-acceptor	3.06	Site gorge wall	
		R247	H-acceptor	3.08	Site gorge wall		
	IV	R463	H-acceptor	3.36	Site gorge wall		
6	BChE	I	W82	π -H	4.36	Ω -loop, PCS	
			W82	π -H	4.43	Ω -loop, PCS	
		III	R515	H-acceptor	3.33	Site gorge wall	
			Q517	H-acceptor	3.14	Site gorge wall	
			Q518	H-acceptor	3.07	Site gorge wall	
		V	Q47	H-acceptor	3.13	Site gorge wall	
			Q176	H-acceptor	3.32	Site gorge wall	

^aBonding interactions, type, and lengths were calculated using built-in Molecular Operating Environment (MOE) 2022.02 features (Chemical Computing Group ULC, Montreal, Quebec, Canada).

^bChE active regions are also denoted, catalytic active site (CAS), peripheral anionic site (PAS), acyl binding pocket (ABP), π -cationic site (PCS), and oxyanion hole (OAH). Docks that did not show any binding interactions are denoted with dashes.